

# 1 Reducing structural uncertainty in conceptual hydrological 2 modelingmodelling in the semi-arid Andes

3  
4 P. HUBLART<sup>1,4</sup>, D. RUELLAND<sup>2</sup>, A. DEZETTER<sup>3</sup> & H. JOURDE<sup>1</sup>

5 <sup>1</sup>UM2, <sup>2</sup>CNRS, <sup>3</sup>IRD – UMR HydroSciences Montpellier, Place E. Bataillon, 34395 Montpellier Cedex 5, France

6 <sup>4</sup>Centro de Estudios Avanzados en Zonas Áridas (CEAZA), Raúl Bitrán s/n, La Serena, Chile

7 [paul.hublart@um2.fr](mailto:paul.hublart@um2.fr) / [denis.ruelland@um2.fr](mailto:denis.ruelland@um2.fr)  
8

9 **Abstract** The use of lumped, conceptual models in hydrological impact studies requires placing more emphasis on the  
10 uncertainty arising from deficiencies and/or ambiguities in the model structure. This study provides an opportunity to  
11 combine a multiple-hypothesis framework with a multi-criteria assessment scheme to reduce structural uncertainty in the  
12 conceptual modelingmodelling of a meso-scale Andean catchment (1515 km<sup>2</sup>) over a 30-year period (1982–2011). The  
13 modelingmodelling process was decomposed into six model-building decisions related to the following aspects of the system  
14 behavior: snow accumulation and melt, runoff generation, redistribution and delay of water fluxes, and natural storage  
15 effects. Each of these decisions was provided with a set of alternative modelingmodelling options, resulting in a total of 72  
16 competing model structures. These structures were calibrated using the concept of Pareto optimality with three criteria  
17 pertaining to streamflow simulations and one to the seasonal dynamics of snow processes. The results were analyzed in the  
18 four-dimensional space of performance measures using a fuzzy *c*-means clustering technique and a differential split sample  
19 test, leading to identify 14 equally acceptable model hypotheses. A filtering approach was then applied to these best-  
20 performing structures in order to minimize the overall uncertainty envelope while maximizing the number of enclosed  
21 observations. This led to retain 8 model hypotheses as a representation of the minimum structural uncertainty that could be  
22 obtained with this modelingmodelling framework. Future work to better consider model predictive uncertainty should include  
23 a proper assessment of parameter equifinality and data errors, as well as the testing of new or refined hypotheses to allow for  
24 the use of additional auxiliary observations.  
25

## 26 1. INTRODUCTION

27 Conceptual catchment models based on the combination of several schematic-interconnected  
28 stores are popular tools in flood forecasting and water resources management (e.g. Jakeman and  
29 Letcher, 2003; Xu and Singh, 2004). The main rationale behind this success lies in the fact that  
30 relatively simple structures with low data and computer requirements generally outweigh the  
31 performance of far more complex physically-based models (e.g. Michaud and Sorooshian, 1994;  
32 Refsgaard and Knudsen, 1996; Kokkonen and Jakeman, 2001). Also, most water management  
33 decisions are made at operational scales having much more to do with catchment-scale administrative  
34 considerations than with our understanding of fine-scale processes. As a result, conceptual models are  
35 being increasingly used to evaluate the potential impacts of climate change on hydrological systems  
36 (e.g. Minville et al., 2008; Ruelland et al., 2012) and freshwater availability (e.g. Milano et al., 2013;  
37 Collet et al., 2013).

38 This modelingmodelling strategy, however, is regularly criticized for oversimplifying the physics  
39 of catchments and leading to unreliable simulations when conditions shift beyond the range of prior  
40 experience. Part of the problem comes from the fact that model structures are usually specified *a*  
41 *priori*, based on preconceived opinions about how systems work, which in general leads to an  
42 excessive dependence on the calibration process. More than a lack of physical background, this  
43 practice reveals a misunderstanding about *how* such models should be based on physics (Kirchner,  
44 2006; Blöschl and Montanari, 2010). Hydrological systems are not structureless things composed of  
45 randomly distributed elements, but rather self-organizing systems characterized by the emergence of  
46 macroscale patterns and structures (Dooge, 1986; Sivapalan, 2006; Ehret et al., 2014). As such, the  
47 reductionist idea that catchments can be understood by merely aggregating (upscaling) fine-scale  
48 mechanistic laws is generally misleading (Dooge, 1997; McDonnell et al., 2007). Self-organization at  
49 the catchment scale means that new hydrologic relationships with fewer degrees of freedom have to be  
50 envisioned (e.g. McMillan, 2012a). Yet, finding simplicity in complexity does not imply that simple  
51 models available in the literature can be used as ready-made engineering tools with little or no  
52 consideration for the specific features of each catchment (Wainwright and Mulligan, 2004; Savenije,  
53 2009). As underlined by Kirchner (2006), it is important to ensure that the “right answers” are  
54 obtained for the “right reasons”. In the case of poorly-defined systems where physically-oriented  
55 interpretations can only be sought *a posteriori* to check for the model realism, this requires placing

56 more emphasis on the uncertainty arising from deficiencies and/or ambiguities in the model structure  
57 than is currently done in most hydrological impact studies.

58 Structural uncertainty can be described in terms of *inadequacy* and *non-uniqueness*. Model  
59 inadequacy arises from the many simplifying assumptions and epistemic errors made in the selection  
60 of which processes to represent and how to represent them. It reflects the extent to which a given  
61 model differs from the real system it is intended to represent. In practice, this results in the failure to  
62 capture all relevant aspects of the system behavior within a single model structure or parameter set. A  
63 common way of addressing this source of uncertainty is to adopt a top-down approach to model-  
64 building (Jothityangkoon et al., 2001; Sivapalan et al., 2003), in which different models of increasing  
65 complexity are tested to determine the adequate level of process representation. Where fluxes and state  
66 variables are made explicit, alternative data sources (other than streamflow) such as groundwater  
67 levels (Seibert, 2000; Seibert and McDonnell, 2002), tracer samples (Son and Sivapalan, 2007; Birkel  
68 et al., 2010; Capell et al., 2012) or snow measurements (Clark et al., 2006; Parajka and Blöschl, 2008),  
69 can also be used to improve the internal consistency of model structures. Additional criteria can then  
70 be introduced in relation to these auxiliary data or to specific aspects of the hydrograph (driven vs.  
71 nondriven components, rising limb, recession limbs...). In this perspective, multi-criteria evaluation  
72 techniques based on the concept of Pareto-optimality provide an interesting way to both reduce and  
73 quantify structural inadequacy (Gupta et al., 1998; Boyle et al., 2000; Efstratiadis and Koutsoyiannis,  
74 2010). A parameter set is said to be Pareto-optimal if it cannot be improved upon without degrading at  
75 least one of the objective criteria. In general, meaningful information on the origin of model  
76 deficiencies can be derived from the mapping of Pareto-optimal solutions in the space of performance  
77 measures (often called the Pareto front) and used to discriminate between several rival structures (Lee  
78 et al., 2011). Further, the Pareto set of solutions obtained with a given model is commonly used to  
79 generate simulation envelopes (hereafter called 'Pareto-envelopes' for brevity's sake) representing the  
80 uncertainty associated with structural errors (i.e. model inadequacy).

81 Non-uniqueness refers to the existence of many different model structures (and parameter sets)  
82 giving equally acceptable fits to the observed data. Structural inadequacy and the limited (and often  
83 uncertain) information of the available data make it highly unlikely to identify a single, unambiguous  
84 representation of how a system works. There may be, for instance, many different possible  
85 representations of flow pathways yielding the same integral signal (e.g. streamflow) at the catchment  
86 outlet (Schaeffli et al., 2011). Non-uniqueness in model identification has also been widely described in  
87 terms of equifinality (Beven, 1993 and 2006) and may be viewed as a special case of a more general  
88 epistemological issue known as the “underdetermination” problem. Over the past decade, these  
89 considerations have encouraged a shift in focus toward more flexible [modelingmodelling](#) tools based  
90 on the concept of multiple working hypotheses (Buytaert and Beven, 2011; Clark et al., 2011). A  
91 number of modular frameworks have been proposed, in which model components (i.e. individual  
92 hypotheses) can be assembled and connected in many ways to build a variety of alternative model  
93 structures (i.e. overall hypotheses). Recent examples of such modular [modelingmodelling](#) frameworks  
94 (MMF) include the Imperial College Rainfall-Runoff [ModelingModelling](#) Toolbox (RRMT) (Wagener  
95 et al., 2002), the Framework for Understanding Structural Errors (FUSE) (Clark et al., 2008) and the  
96 SUPERFLEX [modelingmodelling](#) environment (Fenicia et al., 2011). Clark et al. (2011) suggested  
97 that this approach to model identification represents a valuable alternative to “most practical  
98 applications of the top-down approach”, which “seldom consider competing process representations of  
99 equivalent complexity”. Compared to current multimodel strategies, MMF also provide the possibility  
100 to better scrutinize the effect of each individual hypothesis (i.e. model component), provided that the  
101 model decomposition is sufficiently fine-grained. Finally, Clark et al. (2011) argued that ensembles of  
102 competing model structures obtained from MMF (both of equal and varying complexity) can also be  
103 used to quantify the structural uncertainty arising because of system non-identifiability (i.e. model  
104 non-uniqueness). So far, however, this method has mostly been applied to relatively small (<500 km<sup>2</sup>)  
105 and humid catchments of the Northern Hemisphere (Krueger et al., 2010; Smith and Marshall, 2010;  
106 Staudinger et al., 2011; Kavetski and Fenicia, 2011; McMillan et al., 2012b; Coxon et al., 2013), with  
107 less attention being given to larger scales of interest (>1000 km<sup>2</sup>) and semi-arid regions (e.g. Clark et  
108 al., 2008). Moreover, several of these studies have insisted on the need for multiple criteria related to  
109 different aspects of the system’s behavior in order to improve the usefulness of MMF. Yet, most of the  
110 time these additional criteria or signatures were not used to guide model development or constrain

111 calibration but rather as posterior diagnostics in validation (see Kavetski and Fenicia, 2011). Thus, the  
112 potential benefits of using the concept of Pareto-efficiency to constrain model development and help  
113 differentiate between numerous competing hypotheses remain largely unexplored in the current  
114 literature devoted to MMF. Also, very few studies have included alternative conceptual  
115 representations of snow processes in their modular frameworks (e.g. Smith and Marshall, 2010), even  
116 though snowmelt may have played a significant role in several cases (Clark et al., 2008; Staudinger et  
117 al., 2011).

118 Addressing these issues is of particular importance in the case of arid to semi-arid Andean  
119 catchments such as those found around 30°S. The Norte Chico region of Chile, in particular, has been  
120 identified as being highly vulnerable to climate change impacts in a number of recent reports (IPCC,  
121 2013) and studies (e.g. Souvignet et al., 2010; Young et al., 2010). Yet, very few catchments in this  
122 region have been studied intensively enough to provide reliable model simulations, often with no  
123 estimation of the surrounding uncertainty (Souvignet, 2007; Ruelland et al., 2011; Vicuña et al., 2011;  
124 Hublart et al., 2013). This study is the first step of a larger research project, whose final aim is to  
125 assess the capacity to meet current and future irrigation water requirements in a mesoscale catchment  
126 of the Norte Chico region. The objective here is to provide a set of reasonable model structures that  
127 | can be used for the hydrological ~~modeling~~modelling of the catchment. To achieve this goal, a MMF  
128 was developed and combined with a multi-criteria optimization framework using streamflow and  
129 satellite-based snow cover data.  
130

## 131 2. STUDY AREA

132

133

### 2.1. General site description

134 The Claro River Catchment is a semi-arid, mountainous catchment located in the northeastern part  
135 of the Coquimbo region, in north-central Chile (Fig. 1). It drains an area of approximately 1515 km<sup>2</sup>,  
136 characterized by high elevations ranging from 820 m a.s.l. at the basin outlet (Rivadavia) to over 5500  
137 m a.s.l. in the Andes Cordillera. The topography is dominated by a series of generally north-trending,  
138 fault-bounded mountain blocks interspersed with a few steep-sided valleys.

139 The underlying bedrock consists almost entirely of granitic rocks ranging in age from  
140 Pennsylvanian to Oligocene and locally weathered to saprolite. Above 3000 m a.m.s.l., repeated  
141 glaciations and the continuous action of frost and thaw throughout the year have caused an intense  
142 shattering of the exposed rocks (Caviedes and Paskoff, 1975), leaving a landscape of bare rock and  
143 screes almost devoid of soil.

144 The valley-fill material consists of mostly unconsolidated Quaternary alluvial sediments mantled  
145 by generally thin soils (< 1 m) of sandy to sandy-loam texture. Vineyards and orchards cover most of  
146 the valley floors and lower hill slopes but account for less than 1% of the total catchment area. Most of  
147 the annual precipitation, however, occurs as snow during the winter months, leading to an entire  
148 dependence on surface-water resources to satisfy crop water needs during the summer. Irrigation water  
149 abstractions occur at multiple locations along the river's course depending on both historical water  
150 rights and water availability. By contrast, natural vegetation outside the valleys is extremely sparse and  
151 composed mainly of subshrubs (e.g. *Adesmia echinus*) and cushion plants (e.g. *Laretia acaulis*,  
152 *Azorella compacta*) with very low transpiration rates (Squeo et al., 1993). The Claro River originates  
153 from a number of small tributaries flowing either permanently or seasonally in the mountains.

154

### 155 2.2. Hydro-climatic data

156 | In order to represent the hydro-climate variability of the catchment, a 30-year period (1982–  
157 2011) was chosen according to data availability and quality. Precipitation and temperature data were  
158 interpolated based on respectively 12 and 8 stations (Fig. 1) using the inverse distance weighted  
159 method on a 5km x 5km grid. Since very few measurements were available outside the river valleys,  
160 elevation effects on precipitation and temperature distribution were considered using the SRTM digital  
161 elevation model (Fig. 1). In a previous study, Ruelland et al. (2014) examined the sensitivity of the

162 GR4j hydrological model to different ways of interpolating climate forcing on this basin. Their results  
 163 showed that a dataset based on a constant lapse rate of 6.5°C/km for temperature and no elevation  
 164 effects for precipitation provided slightly better simulations of the discharge over the last 30 years.  
 165 However, since the current study also seeks to reproduce the seasonal dynamics of snow accumulation  
 166 and melt, it was decided to rely on a mean monthly orographic gradient estimated from the  
 167 precipitation observed series (Fig. 1). Potential evapotranspiration (PE) was computed using the  
 168 following formula proposed by Oudin et al. (2005):  
 169

$$PE = \frac{R_e}{\lambda\rho} \times \frac{T + K_2}{K_1} \quad \text{if } T + K_2 > 0 \quad \text{else } PE = 0 \quad (1)$$

170  
 171 where PE is the rate of potential evapotranspiration (mm.d<sup>-1</sup>), R<sub>e</sub> is the extraterrestrial radiation (MJ.m<sup>-2</sup>.d<sup>-1</sup>), λ is the latent heat flux (2.45 MJ.kg<sup>-1</sup>), ρ is the density of water (kg.m<sup>-3</sup>), T is the mean daily air  
 172 temperature (°C) and K<sub>1</sub> and K<sub>2</sub> are fitted parameters (for more details on the values of K<sub>1</sub> and K<sub>2</sub>, see  
 173 Hublart *et al.* (2014)). Water abstractions for irrigation were estimated using information on historical  
 174 water allocations provided by the Chilean authorities. Because these abstractions are likely to  
 175 influence the hydrological behavior of the catchment during recession and low-flow periods, they were  
 176 added back to the gauged streamflow in Rivadavia before calibrating the models. In addition to  
 177 streamflow data, remotely-sensed data from the MODerate resolution Imaging Spectroradiometer  
 178 (MODIS) sensor were used to estimate the seasonal dynamics of snow accumulation and melt  
 179 processes over a 9-year period (2003–2011). Daily snow cover products retrieved from NASA's Terra  
 180 (MOD10A1) and Aqua (MYD10A1) satellites were combined into a single, composite 500-m  
 181 resolution product to reduce the effect of swath gaps and cloud obscuration. The remaining data voids  
 182 were subsequently filled using a linear temporal interpolation method.  
 183

### 184 2.3. Hydrological functioning of the catchment

#### 185 2.3.1. *Precipitation variability*

188 Among the primary factors that control the hydrological functioning of the catchment is the high  
 189 seasonality of precipitation patterns. Precipitation occurs mainly between June and August when the  
 190 South Pacific High reaches its northernmost position. Most of the annual precipitation falls as snow at  
 191 high elevations, where it accumulates in seasonal snow packs that are gradually released from October  
 192 to April. The El Niño Southern Oscillation (ENSO) represents the largest source of climate variability  
 193 at the interannual timescale (e.g. Montecinos and Aceituno, 2003) (Fig. 2). Anomalously wet (dry)  
 194 years in the region are generally associated with warm (cold) El Niño (La Niña) episodes and a  
 195 simultaneous weakening (strengthening) of the South Pacific High. It is worth noting, however, that  
 196 some very wet years in the catchment can also coincide with neutral to weak La Niña conditions, as in  
 197 1984, while several years of below-normal precipitation may not exhibit clear La Niña characteristics  
 198 (Verbist et al., 2010; Jourde et al., 2011). These anomalies may be due to other modes of climate  
 199 variability affecting the Pacific basin on longer timescales. The Interdecadal Pacific Oscillation (IPO),  
 200 in particular, has been shown to modulate the influence of ENSO-related events according to cycles of  
 201 between 15 and 30 years (Quintana and Aceituno, 2012). Recent shifts in the IPO phase occurred in  
 202 1977 and 1998 and may be responsible for the highest frequency of humid years during the 1980s and  
 203 the early 1990s when compared to the late 1990s and the 2000s.

#### 204 2.3.2. *Catchment-scale water balance and dominant processes*

205 Notwithstanding this significant climate variability, a rough estimate of the catchment water  
 206 balance can be given for the period 2003–2011 using the data presented in the previous subsection and  
 207 additional information available in the literature. Spatially averaged precipitation ranges from a ~~low~~  
 208 minimum of 80 mm in 2010 to an estimated high-maximum of 190 mm in 2008. Evapotranspiration  
 209 from non-cultivated areas is sufficiently low to be reasonably neglected at the basin scale (Kalthoff et  
 210 al., 2006). By contrast, water losses from the cultivated portions of the basin are likely to be around 10

211 mm.yr<sup>-1</sup> (Hublart et al., 2014). At high elevations, sublimation plays a much greater role than  
212 evapotranspiration. Mean annual sublimation rates over two glaciers located in similar, neighbouring  
213 catchments have been estimated to be about 1 mm.d<sup>-1</sup> (see e.g. MacDonell et al., 2013). Thus, a first  
214 estimate of the annual water loss associated with snow sublimation can be made by multiplying, for  
215 each day of the period, the proportion of the catchment covered with snow by an average rate of 1  
216 mm.d<sup>-1</sup>. This leads to a mean annual loss of 70 mm between 2003 and 2011. Note that this value is of  
217 the same order of magnitude as those obtained by Favier et al. (2009) using the Weather Research and  
218 Forecasting regional-scale climate model. Mean annual discharge per unit area varies from a minimum  
219 of 20 mm in 2010 to a maximum of 140 mm in 2003. Interestingly, runoff coefficients exceed 100%  
220 during several years of the period (in 2003, 2006, 2007 and 2009), indicating either an underestimation  
221 of precipitation at high elevations, as suggested by Favier et al. (2009), or a delayed contribution of  
222 groundwater to surface flow from one year to another (Jourde et al., 2011).

223 Groundwater movement in the catchment is mainly from the mountain blocks toward the valleys  
224 and then northward along the riverbed. In the mountains, groundwater flow and storage are controlled  
225 primarily by the presence of secondary permeability in the form of joints and fractures (Strauch et al.,  
226 2006). The unconfined valley-fill aquifers are replenished by mountain front recharge along the valley  
227 margins and by infiltration through the channel bed along the losing river reaches (Jourde et al., 2011).  
228 Their hydraulic conductivity and saturated thickness range from about 10 m.d<sup>-1</sup> and 40 m respectively  
229 in the upper part of the catchment to more than 30 m.d<sup>-1</sup> and 60 m respectively at the outlet  
230 (CAZALAC, 2006), allowing a rapid transfer of water to the hydraulically connected surface streams.  
231 Pourrier et al. (2014) studied flow processes and dynamics in the headwaters of the neighbouring  
232 Turbio River catchment; yet very little remains currently known about the emergent processes taking  
233 place at the catchment scale.

234

### 235 3. METHODS

236

#### 237 3.1. Multiple-hypothesis modelingmodelling framework

238 In order to evaluate various numerical representations of the catchment functioning, a multiple-  
239 hypothesis modelingmodelling framework inspired by previous studies in literature was developed.  
240 All the models built within this framework are lumped hypotheses run at a daily time step. The  
241 modelingmodelling process was decomposed into three modules and six model-building decisions.  
242 Each module deals with a different aspect of the precipitation–runoff relationship through one or more  
243 decisions (Fig. 32): snow accumulation (A) and melt (B), runoff generation (C), redistribution (D) and  
244 delay (E) of water fluxes, and natural storage effects (F). Each of these decisions is provided with a set  
245 of alternative modelingmodelling options, which are named by concatenating the following elements:  
246 first a capital letter from A to F referring to the decision being addressed, then a number from 1 to 3 to  
247 distinguish between several competing architectures and, finally, a lower case letter from *a* to *c* to  
248 indicate different parameterizations of the same architecture. Model hypotheses are named by  
249 concatenating the names of the six modelingmodelling options used to build them (see Table 4). The  
250 models designed within this framework share the same overall structure (based on the same series of  
251 decisions) but differ in their specific formulations within each decision.

252 The model-building decisions can be divided into two broad categories. The first pertains to the  
253 production of fluxes from conceptual stores (decisions B, C and F). The second concerns the  
254 allocation and transmission of these fluxes using the typical junction elements and lag functions  
255 (decisions A, D and E) described in Fenicia *et al.* (2011). Junction elements can be defined as “zero-  
256 state” model components used to combine several fluxes into a single one (option D2) or split a single  
257 flux into two or more fluxes (options A1 and D3). Lag functions are used to reflect the travel time  
258 (delay) required to convey water from one conceptual store to another or from one or more conceptual  
259 stores to the basin outlet. They usually consist of convolution operators (option E2), although  
260 conceptual stores may also do the trick. ModelingModelling options in which water fluxes are left  
261 unchanged are labelled as “No operation” options in Fig. 23. Water fluxes and state variables are  
262 named using generic names (from Q1 to Q6 and from S1 to S4, respectively) to ensure a perfect  
263 modularity of the framework. Further details on the alternative options provided for each decision are

264 | given in the following subsections. Note that some combinations of **modelingmodelling** options were  
265 | clearly incompatible with one another (options C1 and C2, for instance, cannot work with option D2).  
266 | As a result, these combinations were removed from the framework.

267 | Another important feature of this modular framework is the systematic smoothing of all model  
268 | thresholds using infinitely differentiable approximants, as recommended by Kavetski and Kuczera  
269 | (2007) and Fenicia *et al.* (2011). The purpose here is twofold: first, to facilitate the calibration process  
270 | by removing any unnecessary (and potentially detrimental) discontinuities from the gradients of the  
271 | objective functions; and second, to provide a more realistic description of hydrological processes  
272 | across the catchment (Moore, 2007).

273

### 274 | *3.1.1. Snow accumulation and melt (decisions A and B)*

275 | Snow accumulation and melt components deal with the representation of snow processes at the  
276 | catchment scale. All **modelingmodelling** options rely on a single conceptual store to accumulate snow  
277 | during the winter months and release water during the melt season. Decision A refers to the  
278 | partitioning of precipitation into rain, snow or a mixture of rain and snow. Decision B refers to the  
279 | representation of snowmelt processes. Option A1 is the only hypothesis implemented to evaluate the  
280 | relative abundance of rain and snow. A logistic distribution is used in this option instead of usual  
281 | temperature thresholds to implicitly account for spatial variations in rain/snow partitioning over the  
282 | catchment. In contrast, three **modelingmodelling** options drawing upon the temperature-index  
283 | approach (Hock, 2003) are available for the evaluation of snowmelt rates (options B1a, B1b, B1c).  
284 | Option B1a relies on a constant melt factor while options B1b and B1c allow for temporal variability  
285 | in the melt factor to reflect seasonal changes in the energy available for melt. A recent example of  
286 | option B1c can be found in Clark *et al.* (2009). Option B1b has been previously applied by Schreider  
287 | *et al.* (1997) but at the grid cell scale. Finally, it is worth noting that a smoothing kernel proposed by  
288 | (Kavetski and Kuczera, 2007) was introduced in the state equation of the snow reservoir to ignore  
289 | residual snow remaining in the reservoir outside the snowmelt season.

290

### 291 | *3.1.2. Runoff generation (decision C)*

292 | Runoff generation components determine how much of a rainfall or snowmelt event is  
293 | available for runoff, lost through evapotranspiration or temporarily stored in soils and surface  
294 | depressions. Many models rely on a conceptual store to keep track of the catchment moisture status  
295 | and generate runoff as a function of both current and antecedent precipitation. Here, an assortment of  
296 | four commonly used methods is available. Option C1 is the only one in which no moisture accounting  
297 | store is required to estimate the contributing rainfall or snowmelt (see Fig. 3). Actual  
298 | evapotranspiration then represents the only process involved in the production of runoff from  
299 | precipitation or snowmelt. The remaining options make use of moisture accounting stores and  
300 | distribution functions (see Table 1) to estimate the proportion of the basin generating runoff. An  
301 | important distinction is made between option C2, in which runoff generation occurs only during  
302 | rainfall or snowmelt events, and option C3, in which a leakage from the moisture accounting store  
303 | remains possible even after rainfall or snowmelt has ceased. Examples of these two moisture  
304 | accounting options can be found, respectively, in the HBV (e.g. Seibert and Vis, 2012) and PDM  
305 | (Moore, 2007) rainfall-runoff models. Alternative distribution functions are available in the literature,  
306 | for instance in the GR4j (Perrin *et al.*, 2003) and FLEX (Fenicia *et al.*, 2008b) models, but the  
307 | rationale behind their use remains the same. Actual evapotranspiration is computed from the estimated  
308 | PE using either a constant coefficient (option C1) or a function of the catchment moisture status  
309 | (options C2 and C3).

### 310 | *3.1.3. Runoff transformation and routing (decisions D to F)*

311 | Runoff transformation components account for all the retention and translation processes  
312 | occurring as water moves through the catchment. In practice, junction elements (decision D) and lag  
313 | functions (decision E) are typically combined with one or more conceptual stores (decision F) to

314 represent the effects of different flow pathways on the runoff process (both timing and volume).  
 315 Additional elements in the form of lag functions or conceptual stores can also be used to reflect water  
 316 routing in the channel network. However, in this study channel routing elements were considered  
 317 | useless at a daily time step. All the [modelingmodelling](#) options available for decision F consist of two  
 318 stores. These can be arranged in parallel (options F1a and F1b), in series (options F2a and F2b), or in a  
 319 combination of both (options F3a and F3b). In each case, one of the stores has a nonlinear behavior  
 320 while the other reacts linearly. Two types of nonlinear response are provided: one that relies on  
 321 smoothed thresholds and different storage coefficients (options F1b, F2b and F3b), and the other that  
 322 relies on power laws (options F1a, F2a and F3a). Options F1a and F1b are based on the classical  
 323 parallel transfer function used in many conceptual models, such as the PDM (Moore, 2007) and  
 324 IHACRES (Jakeman *et al.*, 1993) models, where one store stands for a relatively quick catchment  
 325 response and the other for a slower response. The structure of options F3a and F3b is very close to the  
 326 response routine of the HBV model (e.g. Seibert and Vis, 2012). Note that some combinations of  
 327 | [modelingmodelling](#) options were deemed unacceptable and thus not considered (e.g. D3–E1–F1a or  
 328 D3–E1–F1b).

329  
 330

### 331 3.2. Multi-objective optimization

332  
 333

#### 333 3.2.1. *Principle*

334 In optimization problems with at least two conflicting objectives, a set of solutions rather than  
 335 a unique one exists because of the trade-offs between these objectives. A Pareto-optimal solution is  
 336 achieved when it cannot be improved upon without degrading at least one of its objective criteria. The  
 337 set of Pareto-optimal solutions for a given model is often called the “Pareto set” and the set of criteria  
 338 corresponding to this Pareto set is usually referred to as the “Pareto front”.

339  
 340

#### 340 3.2.2. *The NSGA–II algorithm*

341 The Non-dominated Sorted Genetic Algorithm II (NSGA–II) (Deb, 2002) was selected to  
 342 calibrate the models implemented within the multiple-hypothesis framework. This algorithm has been  
 343 used successfully in a number of recent hydrological studies (see e.g. Khu and Madsen, 2005; Bekele  
 344 and Nicklow, 2007; De Vos and Rientjes, 2007; Fenicia *et al.*, 2008a; Shafii and De Smedt, 2009) and  
 345 has the advantage of not needing any additional parameter (other than those common to all genetic  
 346 algorithms, i.e. the initial population and the number of generations). Its most distinctive features are  
 347 the use of a binary tournament selection, a simulated binary crossover and a polynomial mutation  
 348 operator. For brevity’s sake, the detailed instructions of the algorithm and the conditions of its  
 349 | application to rainfall-runoff [modelingmodelling](#) cannot be discussed further here. Instead, the reader  
 350 is referred to the aforementioned literature.

351  
 352

#### 352 3.2.3. *Simulation periods and assessment criteria*

353 The simulation period was divided into a rather dry calibration period (1997–2011) and a  
 354 relatively humid validation period (1982–1996). These two periods were chosen based on data  
 355 availability to represent contrasted climate conditions: the two periods are separated by a shift in the  
 356 IPO index, as explained in Sect 2.3.1.

357 Four criteria were chosen to evaluate the models built within the multiple-hypothesis  
 358 framework. The first three of them are common to both calibration and validation periods while the  
 359 fourth criterion differs between the two.

360 | The first criterion (NSE) is ~~the~~ related to the estimation of high flows and draws upon the Nash-  
 361 Sutcliffe Efficiency metric:

$$\text{Crit1} = 1 - \text{NSE} = \sum_{d=1}^N (Q_{\text{obs}}^d - Q_{\text{sim}}^d)^2 / \sum_{d=1}^N (Q_{\text{obs}}^d - \overline{Q_{\text{obs}}})^2 \quad (2)$$

362 Where  $Q_{obs}^d$  and  $Q_{sim}^d$  are the observed and simulated discharges for day  $d$ , and  $N$  is the number of  
 363 days with available observations.

364 The second criterion ( $NSE_{log}$ ) is related to the estimation of low flows and draws upon a modified, log  
 365 version of the first criterion:

$$\text{Crit2} = 1 - NSE_{log} = \frac{\sum_{d=1}^N (\log(Q_{obs}^d) - \log(Q_{sim}^d))^2}{\sum_{d=1}^N (\log(Q_{obs}^d) - \log(\overline{Q_{obs}}))^2} \quad (3)$$

366 The third criterion quantifies the mean annual volume error ( $VE_M$ ) made in the estimation of the water  
 367 balance of the catchment:

$$\text{Crit3} = VE_M = \sum_{y=1}^{N_{years}} (|V_{obs}^y - V_{sim}^y| / V_{obs}^y) / N_{years} \quad (4)$$

368 Where  $V_{obs}^y$  and  $V_{sim}^y$  are the observed and simulated volumes for year  $y$ , and  $N_{years}$  is the number of  
 369 years of the simulation period.

370 The fourth criterion (Crit4) differs between the two simulation periods. In calibration, snow-covered  
 371 areas (SCA) estimated from the MODIS data were used to evaluate the consistency of snow-  
 372 accounting **modelingmodelling** options in terms of snow presence or absence at the catchment scale.  
 373 The objective was to quantify the error made in simulating the seasonal dynamics of snow  
 374 accumulation, storage and melt processes. Following Parajka and Blöschl (2008), the snow error (SE)  
 375 was defined as the total number of days when the snow-accounting store of options B1a, B1b and B1c  
 376 disagreed with the MODIS data as to whether snow was present in the basin (Fig. 4). The number of  
 377 days with simulation errors is eventually divided by the total number of days with available MODIS  
 378 data to express SE as a percentage.

379 In validation, a cumulated volume error was used to replace the snow error criterion that could not be  
 380 computed due to a lack of remotely-sensed data over this period:

$$\text{Crit4} = VE_C = \left| \sum_{y=1}^{N_{years}} V_{obs}^y - \sum_{y=1}^{N_{years}} V_{sim}^y \right| / \sum_{y=1}^{N_{years}} V_{obs}^y \quad (5)$$

382

### 383 | 3.3. Model selection, model analysis and ensemble **modelingmodelling**

384 Finally, a total of 72 model structures were implemented and tested within the multi-objective and  
 385 multiple-hypothesis frameworks. In addition to their names and for purposes of simplicity, these 72  
 386 model hypotheses are given a number from 1 to 72 corresponding to their order of appearance in the  
 387 simulation process (see e.g. Sect 4.1.).

388 Model hypotheses can be thought of as points  $x$  in the space of performance measures. One  
 389 possible way to locate these points in space is to consider that each coordinate  $(x_i)_{i=1...4}$  of  $x$  is given  
 390 by the best performance obtained along the Pareto front of model  $x$  with respect to the  $i^{\text{th}}$  criterion  
 391 described in Sect 3.3.2. A clustering technique based on the fuzzy c-means algorithm (Bezdek et al.,  
 392 1983) and the initialization procedure developed by Chiu (1994) was chosen to explore this multi-  
 393 objective space and identify natural groupings among model hypotheses. To facilitate comparison  
 394 between calibration and validation, the clustering operations were repeated independently for each  
 395 period. The whole experiment, from model building to multi-objective optimization and cluster  
 396 identification, was repeated several times to ensure that the final composition of the clusters remains  
 397 the same.

398 Once the composition of each cluster was established, it was possible to identify a set of ‘best-  
 399 performing’ clusters for each simulation period, i.e. a set of clusters with the smallest Euclidian  
 400 distances to the origin of the objective space. The model structures of these ‘best-performing’ clusters  
 401 can be regarded as equally acceptable representations of the system. An important indicator of

402 structural uncertainty is the extent to which the simulation bounds derived from the Pareto sets of  
 403 these models reproduce the various features of the observed hydrograph. The overall uncertainty  
 404 envelope should be wide enough to include a large proportion of the observed discharge but not so  
 405 wide that its representation of the various aspects of the hydrograph (rising limb, peak discharge,  
 406 falling limb, baseflow) becomes meaningless. In this study, priority was given to maintaining at its  
 407 lowest value the number of outlying observations before searching for the best combination of models  
 408 which minimized the envelope area. This was achieved iteratively through the following steps:

- 410 1. Start with an initial ensemble composed of the  $N_{max}$  models identified as members of the  
 411 best-performing clusters in both calibration and validation (i.e. models which fail the  
 412 validation test are ruled out).
- 413 2. From now on, consider only the calibration period.  
 414 Add up the  $N_{max}$  individual simulation envelopes that can be obtained from the Pareto sets of  
 415 the  $N_{max}$  models (hereafter referred to as the ‘Pareto-envelopes’).
- 416 3. Estimate the maximum number of observations enclosed within the resulting overall envelope,  
 417  $N_{obs}(N_{max})$ , and calculate the area of this envelope,  $Area(N_{max})$ .
- 418 4. For  $k = 1$  to  $N_{max}$ 
  - 419 a. Identify the  $\binom{N_{max}}{N_{max} - k}$  possible combinations of  $N_{max}$  models taken  $N_{max} - k$  at a time.
  - 420 b. For each of these combinations
    - 421 - Add up the individual Pareto-envelopes of the  $N_{max} - k$  models and calculate the  
 422 number of observations enclosed within the bounds of the resulting overall envelope,  
 423  $N_{obs}(N_{max} - k)$ .
    - 424 - If  $N_{obs}(N_{max} - k) = N_{obs}(N_{max})$   
 425 If  $Area(N_{max} - k) < Area(N_{max} - k + 1)$   
 426 Accept the current combination.
    - 427 If  $N_{obs}(N_{max} - k) < N_{obs}(N_{max})$   
 428 Reject the current combination.
  - 429 c. If all the possible combinations of  $N_{max} - k$  models are rejected, break the loop. The final  
 430 ensemble of models to consider is the last accepted combination of  $N_{max} - k + 1$  models.  
 431

## 432 4. RESULTS

433

434

### 4.1. Model hypotheses evaluation

435

436

#### 4.1.1. Cluster analysis

437 The 72 model hypotheses can be grouped into 5 clusters in calibration and 6 in validation. Table 3  
 438 displays the coordinates of the cluster centroids and gives, for each cluster, the number of points with  
 439 membership values above 50%. Figure 5 shows the projections of these clusters onto three possible  
 440 two-dimensional (2D) subspaces of the objective space (the three other subspaces being omitted for  
 441 brevity's sake). Each cluster is given a rank (from 1 to 5 or 6) reflecting its distance from the origin of  
 442 the coordinate system. As is evident from both Fig. 5 and Table 3, most of the best-performing  
 443 structures can be found in Cluster 1. This is particularly clear in the planes defined by the high-flow  
 444 (Crit1) and low-flow (Crit2) criteria (Figure 5), where all clusters tend to line up along a diagonal axis  
 445 (dashed line). In contrast, a small trade-off between Cluster 1 and Cluster 2 can be observed in  
 446 calibration in the plane defined by the high-flow (Crit1) and volume error (Crit3) criteria: models from  
 447 Cluster 2 (respectively Cluster 1) tend to perform slightly better than those from Cluster 1  
 448 (respectively Cluster 2) with respect to Crit3 (respectively Crit1). However, this trade-off disappears  
 449 in validation. Similar comments can be made about the other 2D subspaces (not shown here). In the  
 450 following analysis, Cluster 1 will be considered as the only best-performing cluster. This cluster  
 451 encompasses 24 members in calibration as against 15 in validation, indicating that several model  
 452 structures do not pass the validation test (namely models no. 30, 32, 49, 52, 53, 55, 66, 67, 69 and 72,  
 453 as shown in Table 4).

454 Several observations can be made regarding the composition of Cluster 1 in both simulation  
455 periods. As can be seen from the values listed in Table 4, it is not possible to pick out a single,  
456 unambiguous model hypothesis that would perform better than the others with respect to all criteria.  
457 On the one hand, there appears to be several equally acceptable structures for each individual criterion.  
458 Models no. 22 (A1–B1a–C3–D2–E1–F2b), 46 (A1–B1b–C3–D2–E1–F2b) and 54 (A1–B1c–C1–D3–  
459 E2–F1b), for instance, yield very similar values of the high-flow criterion (Crit1), despite some  
460 differences in their **modelingmodelling** options. This illustrates the equifinality of model structures in  
461 reproducing one aspect of the system behavior. On the other hand, some structures seem more  
462 appropriate to the simulation of high flows or snow dynamics while others appear to be better at  
463 reproducing low flows or estimating the annual water balance of the catchment. This indicates trade-  
464 offs between model structures in reproducing several aspects of the system behavior. It is however  
465 possible to identify some recurring patterns among the **modelingmodelling** options present in (or  
466 absent from) Cluster 1 in both periods. First, option B1c is the most represented snowmelt-accounting  
467 hypothesis, despite an increase in the number of alternative options (B1a, B1b) in validation. More  
468 strikingly, option C2 is totally absent from Cluster 1 in both periods. Single-flux combinations (C1–  
469 D1 and C3–D2) and their splitting counterparts (C1–D3 and C3–D1) tend to be equally well-  
470 represented, thus providing evidence of significant equifinality among these conceptual  
471 representations. Finally, runoff transformation options based on a threshold-like behavior (F1b, F2b  
472 and F3b) account for 75% of model hypotheses in calibration and over 90% in validation. In  
473 particular, option F3a turns out to be completely absent from Cluster 1 in both periods while models  
474 based on option F2a (no. 49, 55, 67 and 69) fail the validation test. On the opposite, option F2b is  
475 particularly well-represented.

476  
477

#### 4.1.2. Pareto analysis

478 In general, valuable insight can be gained from the mapping of Pareto fronts in the space of  
479 performance measures. While a full description of all the Pareto fronts obtained in calibration is not  
480 possible here due to space limitations, two model hypotheses are used to illustrate this point. Figure 6  
481 shows the Pareto-optimal solutions of models no. 49 (A1–B1c–C1–D1–E1–F2a) and 50 (A1–B1c–  
482 C1–D1–E1–F2b) plotted in two dimensions for different combinations of two of the four objective  
483 functions used in calibration. Note that these two models differ only in their runoff transformation  
484 options (F2a vs. F2b) so that the comparison can be made in a controlled way. Trade-offs between the  
485 high-flow (Crit1) and low-flow (Crit2) criteria are clearly more important with option F2a (Fig. 6a)  
486 than with option F2b (Fig. 6b). This means that option F2a is less efficient in reproducing  
487 simultaneously high and low flows and explains why this option disappears from Cluster 1 in  
488 validation. By contrast, the other pairs of criteria (Crit1–Crit3, Crit1–Crit4) displayed in Fig. 6 appear  
489 to be less useful in differentiating between the two models.

490 Further insight into the structural strengths and weaknesses of model hypotheses can be  
491 obtained by determining how parameter values vary along the Pareto fronts of the models. A large  
492 'Pareto range' in some parameters indicates structural deficiencies in the corresponding model  
493 components (see e.g. Gupta *et al.*, 1998) or a lower sensitivity of model outputs to those parameters  
494 (Engeland *et al.*, 2006). For purposes of clarity, Fig. 7 focuses on eight illustrative structures identified  
495 as members of Cluster 1 in calibration. The models are paired in such a way that two models of the  
496 same pair differ in only one **modelingmodelling** option. Thus, the effects of potential interactions  
497 between model constituents are more likely to be detected. Parameter values are normalized using the  
498 lower and upper limits given in Table 2 so that all of them lie between 0 and 1. Different colors are  
499 used to indicate the parameter sets associated with the smallest high-flow (in black), low-flow (in red),  
500 volume (in blue) and snow (in green) errors. ~~To what extent~~ The extent to which these colored  
501 solutions converge toward the same parameter values or diverge from each other determines the level  
502 of parameter identifiability of each model hypothesis. ~~As regards~~ In terms of snow-accounting options,  
503 a distinction can be made between snow accumulation parameters ( $T_S$  and  $m_S$ ), whose ranges of  
504 variation appear to be large in all cases, and snowmelt parameters ( $T_M$ ,  $f_M$ ,  $r_1$ ,  $r_2$ ,  $f_1$ ,  $f_2$ ), whose levels  
505 of identifiability depend on interactions with the other model components. In Fig. 7a, the Pareto range  
506 of snowmelt parameters decreases in width when moving from option B1a to B1b and using the  
507 combination of options C3–D2–E1. Yet changing this combination into C3–D1–E2 has the opposite

508 | effect (Fig. 7b): parameter uncertainty now decreases when moving from option B1b to B1a. As  
509 | regardsIn terms of runoff transformation parameters ( $\alpha$ ,  $N_b$ ,  $K_2$ ,  $K_3$ ,  $\delta$ ,  $S_C$  and  $K_4$ ), the black and red  
510 | solutions are closer to each other when options F2b (Fig. 7a, 7b and 7c) and F1b (Fig. 7d) are used. By  
511 | contrast, options F2a (Fig. 7c) and F1a (Fig. 7d) require very different parameter sets to adequately  
512 | simulate both low and high flows. Again, this suggests that runoff transformation options based on a  
513 | threshold-like behavior may be more consistent with the observed data than those based on a power  
514 | law relationship. It should be noted, however, that relatively large Pareto ranges in some runoff  
515 | transformation parameters (e.g.  $K_2$  and  $K_3$ ) may still be required to obtain small volume and snow  
516 | errors at the same time as high low-flow and high-flow performances (e.g. models no. 44 and 54).  
517 | Interestingly, the black, red and blue solutions of models no. 49, 50, 53 and 54 also converge towards  
518 | the same low values of parameter  $K_C$  (evapotranspiration coefficient) independently of runoff  
519 | transformation options.

520 | Drawing any conclusion at this stage about the links between parameter identifiability and model  
521 | performance might be somewhat hazardous. Other examples (not shown here) show that a model  
522 | structure may have highly identifiable parameter values in calibration and yet not be suited to the  
523 | conditions prevailing in validation. Also, a reduction of parameter uncertainty as is the case with  
524 | options F2b and F1b often comes with a greater number of parameters.

525 | Finally, a better understanding of the reasons why some models, or modelingmodelling  
526 | options, work better than others is provided by the simulation bounds (or Pareto-envelopes) derived  
527 | from the Pareto sets of these models. Figure 8 shows the Pareto-envelopes of the SWE internal state  
528 | variable obtained with three competing model hypotheses (no. 6, 30 and 54) differing only in their  
529 | snowmelt-accounting options (respectively B1a, B1b and B1c). Note that only the last two of these  
530 | models (30, 54) belong to Cluster 1 in calibration (see Table 4). Simulated snow accumulation starts  
531 | later than expected with all modelingmodelling options (B1a, B1b and B1c). As will be further  
532 | discussed in Sect 5.2., this is likely to indicate systematic errors in the input precipitation and/or  
533 | MODIS-based SCA data. On the whole, the envelope widths suggest a reduction in the uncertainty  
534 | associated with the prediction of snow seasonal dynamics when moving from option B1a to option  
535 | B1c. This is consistent with the mean annual snow errors reported in Table 4, which are significantly  
536 | lower with option B1c independently of the other model options. It must be acknowledged, however,  
537 | that even this option (B1c) fails to capture the seasonal dynamics of snow accumulation and melt  
538 | during several years of the period. The release of water from the snow-accounting store of model no.  
539 | 54 continues well after the end of the observed snowmelt season in 2008, 2009, 2010 and 2011. On the  
540 | contrary, the simulated snowmelt season tends to end sooner than expected with model no. 30 in 2003,  
541 | 2004, 2005 and 2006. In that case, options B1b and B1c appear to be somewhat complementary.

542

543

#### 4.2. Representation of structural uncertainties

544 | This Section deals with the identification and use of an ensemble of equally acceptable model  
545 | structures to quantify and represent the uncertainty arising from the system non-identifiability. Figure  
546 | 9 shows the overall uncertainty envelope obtained with the 8 model structures whose combination  
547 | minimizes the envelope area in calibration while holding constant the number of outlying observations  
548 | (see Sect 3.3.). Over 82% of discharge observations are captured by the envelope in both simulation  
549 | periods. Interestingly, this number exceeds the best  $N_{\text{par}}$  value obtained in calibration with the  
550 | individual Pareto-envelopes (see Table 4), which shows how necessary it is to consider an ensemble of  
551 | model structures. In validation, however, a better combination could be identified since several models  
552 | of Cluster 1 display significantly higher  $N_{\text{par}}$  values (Table 4). On the whole, the comparison of the  
553 | observed hydrograph with the simulation bounds of the envelope shows a good match of rising limbs  
554 | and peak discharges in both simulation periods, but a less accurate fit of falling limbs during at least  
555 | one major (in 1987–88) and two minor (in 2005–06 and 2007–08) events. The slower recession of the  
556 | observed hydrograph might indicate a delayed contribution of one or more catchment compartments  
557 | that cannot be described by any of the modelingmodelling options available in the multiple-hypothesis  
558 | framework.

559

560

561 **5. DISCUSSION & CONCLUSION**  
562

563 | This study aimed at reducing structural uncertainty in the [modelingmodelling](#) of a semi-arid Andean  
564 | catchment where lumped conceptual models remain largely under-used. To overcome the current lack  
565 | of information on model adequacy in this catchment, a modular [modelingmodelling](#) framework  
566 | (MMF) relying on six model-building decisions was developed to generate 72 competing model  
567 | structures. Four assessment criteria were then chosen to calibrate and evaluate these models over a 30-  
568 | year period using the concept of Pareto-optimality. This strategy was designed to characterize both the  
569 | parameter uncertainty arising from each model's structural deficiencies (i.e. model inadequacy) and the  
570 | ambiguity associated with the choice of model components (i.e. model non-uniqueness). Finally, a  
571 | clustering approach was taken to identify natural groupings in the multi-objective space. Overall, the  
572 | greatest source of uncertainty was found in the connection between runoff generation and runoff  
573 | transformation components (decisions D and E). However, the results also showed a significant drop  
574 | in the number of plausible representations of the system. After validation, 14 model structures among  
575 | the 24 identified in calibration as the best-performing ones were finally considered as equally  
576 | acceptable.

577  
578 | [5.1. Improved understanding of hydrological processes](#)  
579

580 | Interestingly, both rejected and accepted hypotheses appeared closely related to particular types of  
581 | snowmelt-accounting (decision B), runoff generation (decision C) and runoff transformation (decision  
582 | D) [modelingmodelling](#) options, suggesting possible links to some physical features of the catchment.  
583 | For instance, the frequent occurrence of option C1 and the absence of option C2 among the set of best-  
584 | performing structures indicate that moisture-accounting components may not be essential to the  
585 | conceptual [modelingmodelling](#) of this catchment. Most of the land cover is, indeed, dominated by  
586 | barren to sparsely vegetated exposed rocks, boulders and rubble with poor soil development outside  
587 | the valleys. This setting may also explain the relatively low values of parameter  $K_C$  obtained with the  
588 | black, red and blue solutions shown in Fig. 76. Likewise, the frequency of options F2a and F2b in the  
589 | best-performing cluster suggests that the catchment actually behaves as a ‘serial’ system. The overall  
590 | organization of fluxes in the catchment, from high elevations toward the valleys and then northward to  
591 | the outlet, can be conceptualized as a series of two hydraulically connected reservoirs: one standing  
592 | for the granitic mountain blocks (upstream reservoir) and the other for the alluvial valleys  
593 | (downstream reservoir). Similar results were also obtained for smaller catchments in Luxembourg  
594 | characterized by relatively impervious bedrocks and lateral water flows (Fenicia et al., 2014). The  
595 | results also provided some evidence of a strong threshold behavior at the catchment scale (options  
596 | F1b, F2b and F3b) compared to the smoother power laws of options F1a, F2a and F3a. However,  
597 | further research would be needed to track the origin of this behavior, which might be related at some  
598 | point to connectivity levels in the fractured and till-mantled areas of the mountain blocks. As regards  
599 | snowmelt, the frequent occurrence of option B1c in the best-performing cluster in calibration may  
600 | indicate a need to account for processes which the degree-day method implemented in option B1a does  
601 | not fully capture. In semi-arid central Andes (29–30°S), small zenith angles and a thin, dry and cloud-  
602 | free atmosphere during most of the year make incoming shortwave radiation the most important  
603 | source of seasonal variations in the energy available for melt (e.g. Pellicciotti et al., 2008; Abermann  
604 | et al., 2013). While this dominant source of energy cannot be accounted for by temperature alone, the  
605 | seasonal timing of snowmelt is also expected to show a greater year-to-year stability, which may  
606 | explain the relative success of option B1c when compared to option B1b.

607 | Of course, these hypothesized relationships between some physical characteristics of the  
608 | catchment and specific [modelingmodelling](#) options need to be further qualified. Differentiating  
609 | between physically adequate and purely numerical solutions will always seem somewhat hazardous in  
610 | the case of lumped conceptual models. For instance, a small number of models among those identified  
611 | as the best-performing ones also rely on parallel (F1a, F1b) and intermediate (F3b) runoff  
612 | transformation options. Also, the relative proportions of snowmelt-accounting options B1a, B1b and  
613 | B1c, appears much more balanced in validation, where no snow error criterion could be applied, than  
614 | in calibration. Although this was not our objective in this paper, comparative studies including several

615 similar or contrasted catchments would be required to better understand how different model  
616 structures relate to different physical settings. Such understanding is of primary importance to the  
617 choice of conceptual models in climate change impact studies.

### 618 5.2. Model parsimony

619  
620  
621 Another important issue related to model identification is the extent to which the 'principle of  
622 parsimony' can be applied to differentiate between a large number of model hypotheses. Many authors  
623 rightly consider that a maximum of 5 to 6 parameters should be accepted in calibration when using a  
624 single objective function. Efstratiadis and Koutsoyiannis (2010) extended this empirical rule to the  
625 case of multi-objective schemes by allowing « a ratio of about 1:5 to 1:6 between the number of  
626 criteria and the number of parameters to optimize ». For a multi-objective scheme based on four  
627 criteria (as in the present study), this leads to consider 20 to 24-parameter models as still being  
628 parsimonious. This will certainly seem unreasonable to many modelers because, as Efstratiadis and  
629 Koutsoyiannis (2010) also pointed out, the various criteria used are generally not independent of each  
630 other. In our case, for instance, the information added by the low-flow criterion may not be so  
631 different from that already introduced by the high-flow criterion. By contrast, the snow criterion tends  
632 to add new information on the snow-related parameters. From this perspective, it is noteworthy that  
633 most rejected hypotheses among the 24 identified in calibration as members of Cluster 1 had more  
634 than 11 free parameters, with only one having 9 parameters. The principle of parsimony, however,  
635 cannot be used to further discriminate between the remaining 14 best-performing hypotheses. For  
636 instance, model no. 54 (12 parameters) performs better than model no. 2 (9 parameters) with respect to  
637 the high-flow criterion.

### 638 5.3. Uncertainty quantification

639  
640  
641 Eventually, the number of models used to represent structural uncertainty was reduced by  
642 searching for which minimal set of models maximized the number of observations covered by the  
643 ensemble of Pareto-envelopes. It is important to make clear that model inadequacy and non-  
644 uniqueness were evaluated here in non-probabilistic terms. In particular, the Pareto-envelopes derived  
645 for each model structure quantify only the uncertainty arising from the trade-offs between competing  
646 criteria and do not have a predefined statistical meaning (Engeland et al., 2006). Consequently, the  
647 overall simulation bounds shown in Figure 89 cannot be easily interpreted as 'confidence bands'.  
648 Although discussing the adequacy of non-probabilistic approaches to structural uncertainty was far  
649 beyond the scope of this study, it is interesting to analyze the reasons why between 15% and 20% of  
650 the observations remained outside the overall simulated envelope in both calibration and validation.  
651 To a large extent, this lack of performance can be attributed either to an insufficient coverage of the  
652 hypothesis and objective spaces or to uncertainties in the precipitation and streamflow data that were  
653 overlooked in this study.

654 ~~First,~~ The choice of Pareto-optimality to characterize structural uncertainty can be criticized for  
655 leading to the rejection of many behavioral parameter sets (i.e. being close to, but not part of, the  
656 Pareto front) that might have been Pareto-optimal with different performance measures, calibration  
657 data or input errors (e.g. Freer et al., 2003; Beven, 2006). Also, this concept should not be confused  
658 with that of equifinality. Both notions agree that it is not possible to identify a single, best solution to  
659 the calibration problem and that multiple parameters sets should be retained to give a proper account  
660 of model uncertainty. However, the Pareto set of solutions represents the minimum parameter  
661 uncertainty that can be achieved when several criteria are considered simultaneously with no *a priori*  
662 preference for one over the others (Gupta et al., 2003). By contrast, two parameter sets are said to be  
663 equifinal (in a statistical sense) if they can be regarded as equally acceptable with respect to a given  
664 model outcome. For a proper assessment of parameter equifinality, more probabilistic approaches  
665 should be taken (Madsen, 2000; Huisman *et al.*, 2010). In the context of multiple-hypothesis testing, a  
666 meticulous selection of the assessment criteria is also critical to avoid rejecting some  
667 ~~modeling~~ modelling options for the wrong reasons. For instance, the snow error criterion was shown to  
668 have a great influence on the identification of snow-accounting components, as much more ambiguity  
669 between the various available options was observed during the validation period when this criterion

670 could not be used. Also, like any other multiple-hypothesis framework, the MMF developed in this  
671 study suffers from an insufficient coverage of the hypothesis space (Gupta et al., 2012). The  
672 parameterization of evapotranspiration, for example, was not considered as an independent model-  
673 building decision. Only one formula was applied to calculate potential evapotranspiration and the  
674 possibility to retrieve actual evapotranspiration from downstream water stores was not provided.  
675 Likewise, the runoff transformation process was described using only two water stores, of which only  
676 one was assumed to have a nonlinear behavior. Future work to improve the conceptual  
677 **modelingmodelling** of the Claro River catchment should include the testing of new or refined  
678 hypotheses to allow for the use of additional auxiliary data (e.g. observed snow heights, irrigation  
679 water-use).

#### 681 5.4. Data quality issues

682  
683 More fundamentally, our ability to discriminate among the competing model hypotheses was  
684 constrained by inevitable errors in the input and output data sets. In particular, the comparison of  
685 simulated SWE levels and MODIS-based SCA estimates revealed some uncertainty in the estimation  
686 of precipitation inputs and confirmed previous results obtained by Favier et al. (2009). Some  
687 precipitation events occurring in the early winter may not be captured by the gauging network (< 3200  
688 m a.s.l.) used for the interpolation of precipitation across the catchment. These errors may add to  
689 systematic volume errors caused by wind, wetting and evaporation losses at the gauge level, leading to  
690 an overall underestimation of precipitation, as indicated by the rough estimate of the catchment-scale  
691 water balance given in Sect 2. It was also possible to highlight some errors in the streamflow data. The  
692 observed streamflow was ‘naturalized’ by simply adding back the estimated historical water  
693 abstractions (Sect. 2.2). When applied on a daily basis, this process inevitably adds some uncertainty  
694 to streamflow values because a significant part of surface-water abstractions actually return to the river  
695 system within a few days due to conveyance and field losses. In general, ignoring these return flows  
696 would lead to overestimating daily natural flows. In this paper, however, the actual water withdrawals  
697 were not known with precision but only as percentages of the nominal water rights – these percentages  
698 being fixed on a monthly basis by the authorities to account for variations in water availability. The  
699 combined impact of streamflow and precipitation errors on the assessment of structural uncertainty  
700 thus remained unknown. Further research is currently underway to integrate the effects of water  
701 abstractions and crop water-use in the hydrological **modelingmodelling** process (Hublart et al., 2015;  
702 see also Kiptala et al., 2014 for another approach). From a multiple-hypothesis perspective, the  
703 **modelingmodelling** of irrigation water-use should be regarded as a testable model component in its  
704 own right.  
705

706 **Acknowledgements** The authors are very grateful to the Centro de Estudios Avanzados en Zonas  
707 Áridas (CEAZA) for its essential logistic support during the field missions and to Gustavo Freixas  
708 from the *Dirección General de Agua* (Chile) for providing the necessary streamflow data. The authors  
709 also thank S. Lhermitte, D. López and S. MacDonell for providing the MODIS data used in this study  
710 and S. Gascoin for informal advice and much useful discussion. Moreover, the authors thank the two  
711 anonymous reviewers for their interest to this work and for their useful comments that helped to  
712 improve the article.

713

#### 714 **REFERENCES**

- 715 Abermann, J., Kinnard, C., and MacDonell, S.: Albedo variations and the impact of clouds on glaciers in the  
716 Chilean semi-arid Andes, *J. Glaciol.*, 60, 183–191, 2013.
- 717 Bekele, E. G. and Nicklow, J. W.: Multi-objective automatic calibration of SWAT using NSGA-II, *J. Hydrol.*,  
718 341, 165–176, 2007.
- 719 Beven, K.: Prophecy, reality and uncertainty in distributed hydrological modelling, *Adv. Water Resour.*, 16, 41–  
720 51, 1993.

- 721 Beven, K.: A Manifesto for the Equifinality Thesis, *J. Hydrol.*, 320, 18–36, 2006.
- 722 Bezdek, J. C., Ehrlich, R., and Full, W.: FCM: The fuzzy c-means clustering algorithm, *Comput. Geosci.*, 10,  
723 191–203, 1983.
- 724 Birkel, C., Tetzlaff, D., Dunn, S. M., and Soulsby, C.: Towards a simple dynamic process conceptualization in  
725 rainfall–runoff models using multi-criteria calibration and tracers in temperate, upland catchments. *Hydrol.*  
726 *Process.*, 24, 260–275, doi: 10.1002/hyp.7478, 2010.
- 727 Blöschl, G. and A. Montanari: Climate change impacts–throwing the dice?, *Hydrol. Process.*, 24, 374–381, 2010.
- 728 Boyle, D. P., Gupta, H. V., and Sorooshian, S.: Toward improved calibration of hydrologic models: Combining  
729 the strengths of manual and automatic methods, *Water Resour. Res.*, 36, 3663–3674,  
730 doi:10.1029/2000WR900207, 2000.
- 731 Buytaert, W. and K. Beven: Models as multiple working hypotheses: hydrological simulation of tropical alpine  
732 wetlands, *Hydrol. Process.*, 25, 1784–1799, 2011.
- 733 Capell, R., Tetzlaff, D., and Soulsby, C.: Can time domain and source area tracers reduce uncertainty in  
734 rainfall–runoff models in larger heterogeneous catchments?, *Water Resour. Res.*, 48, W09544,  
735 doi:10.1029/2011WR011543, 2012.
- 736 Caviedes, C. N. and Paskoff, R.: Quaternary glaciations in the Andes of north-central Chile, *J. Glaciol.*, 14, 155–  
737 169, 1975.
- 738 Centro del Agua para Zonas Áridas y semiáridas de América Latina y el Caribe (CAZALAC): Aplicación de  
739 metodologías para determinar la eficiencia de uso del agua – Estudio de caso en la Región de Coquimbo.  
740 Informe Técnico, Gobierno Regional, Santiago (Chile), 2006.
- 741 Chiu, S.: Fuzzy model identification based on cluster estimation, *J. Intell. Fuzzy Syst.*, 2, 267– 278, 1994.
- 742 Clark, M. P., Slater, A. G., Barrett, A. P., Hay, L. E., McCabe, G. J., Rajagopalan, B., and Leavesley, G. H.:  
743 Assimilation of snow covered area information into hydrologic and landsurface models, *Adv. Water*  
744 *Resour.*, 29, 1209–1221, 2006.
- 745 Clark, M. P., Slater, A. G., Rupp, D. E., Woods, R. A., Vrugt, J. A., Gupta, H. V., Wagener, T., and Hay, L. E.:  
746 Framework for Understanding Structural Errors (FUSE): A modular framework to diagnose differences  
747 between hydrological models, *Water Resour. Res.*, 44, W00B02, doi:10.1029/2007WR006735, 2008.
- 748 Clark, M., Hreinsson, E. O., Martinez, G., Tait, A., Slater, A., Hendrikx, J., Owens, I., Gupta, H., Schmidt, J., and  
749 Woods, R.: Simulations of seasonal snow for the South Island, New Zealand, *J. Hydrol.*, 48, 41–58, 2009.
- 750 Clark, M. P., Kavetski, D., and Fenicia, F.: Pursuing the method of multiple working hypotheses for hydrological  
751 [modelingmodelling](#), *Water Resour. Res.*, 47, W09301, doi:10.1029/2010WR009827, 2011.
- 752 Collet, L., Ruelland, D., Borrell-Estupina, V., Dezetter, A., and Servat, E.: Integrated modelling to assess long-  
753 term water supply capacity of a meso-scale Mediterranean catchment, *Sci. Total Environ.*, 461–462, 528–  
754 540, 2013.
- 755 Coxon, G., Freer, J., Wagener, T., Odoni, N. A., and Clark, M. P.: Diagnostic evaluation of multiple hypotheses  
756 of hydrological behaviour in a limits-of-acceptability framework for 24 UK catchments, *Hydrol. Process.*,  
757 doi:10.1002/hyp.10096, online first, 2013.
- 758 De Vos, N. J., and Rientjes, T. H. M.: Multi-objective performance comparison of an artificial neural network  
759 and a conceptual rainfall–runoff model, *Hydrolog. Sci. J.*, 52, 397–413, doi: 10.1623/hysj.52.3.397, 2007.
- 760 Deb, K., Pratap, A., Agarwal, S., and Meyarivan, T.: A fast and elitist multiobjective genetic algorithm: NSGA-II,  
761 *IEEE T. Evolut. Comput.*, 6, 181–197, 2002.
- 762 Dooge, J.: Looking for hydrologic laws, *Water Resour. Res.*, 22, 46S–58S, doi:10.1029/WR022i09Sp0046S,  
763 1986.
- 764 Dooge, J.: Searching for Simplicity in Hydrology, *Surv. Geophys.*, 18, 511–534, 1997.
- 765 Efstratiadis, A., and Koutsoyiannis, D.: One decade of multi-objective calibration approaches in hydrological  
766 modelling: a review, *Hydrolog. Sci. J.*, 55, 58–78, 2010.
- 767 Ehret, U., Gupta, H. V., Sivapalan, M., Weijjs, S. V., Schymanski, S. J., Blöschl, G., Gelfan, A. N., Harman, C.,  
768 Kleidon, A., Bogaard, T. A., Wang, D., Wagener, T., Scherer, U., Zehe, E., Bierkens, M. F. P., Di  
769 Baldassarre, G., Parajka, J., van Beek, L. P. H., van Griensven, A., Westhoff, M. C., and Winsemius, H. C.:

- 770 Advancing catchment hydrology to deal with predictions under change, *Hydrol. Earth Syst. Sci.*, 18, 649–  
771 671, doi:10.5194/hess-18-649-2014, 2014.
- 772 Engeland, K., Braud, I., Gottschalk, L., and Leblois, E.: Multi-objective regional modelling, *J. Hydrol.*, 327,  
773 339–351, 2006.
- 774 Favier, V., Falvey, M., Rabatel, A., Praderio, E., and López, D.: Interpreting discrepancies between discharge and  
775 precipitation in high-altitude area of Chile's Norte Chico region (26–32°S), *Water Resour. Res.*, 45,  
776 W02424, doi:10.1029/2008WR006802, 2009.
- 777 Fenicia, F., McDonnell, J. J., and Savenije, H. H. G.: Learning from model improvement: On the contribution of  
778 complementary data to process understanding, *Water Resour. Res.*, 44, W06419,  
779 doi:10.1029/2007WR006386, 2008a.
- 780 Fenicia, F., Savenije, H. H. G., Matgen, P., and Pfister, L.: Understanding catchment behavior through stepwise  
781 model concept improvement, *Water Resour. Res.*, 44, W01402, doi:10.1029/2006WR005563, 2008b.
- 782 Fenicia, F., Kavetski, D., and Savenije, H. H. G.: Elements of a flexible approach for conceptual hydrological  
783 [modelingmodelling](#): I. Motivation and theoretical development, *Water Resour. Res.*, 47, W11510,  
784 doi:10.1029/2010WR010174, 2011.
- 785 Fenicia, F., Kavetski, D., Savenije, H. H. G., Clark, M. P., Schoups, G., Pfister, L., and Freer, J.: Catchment  
786 properties, function, and conceptual model representation: is there a correspondence?, *Hydrol. Process.*,  
787 28, 2451–2467, doi: 10.1002/hyp.9726, 2014.
- 788 Freer, J., Beven, K., and Peters, N.: Multivariate Seasonal Period Model Rejection Within the Generalised  
789 Likelihood Uncertainty Estimation Procedure, in *Calibration of Watershed Models* (eds Q. Duan, H. V.  
790 Gupta, S. Sorooshian, A. N. Rousseau and R. Turcotte), American Geophysical Union, Washington, D. C.,  
791 69–87, 2003.
- 792 Gupta, H. V., Sorooshian, S., and Yapo, P. O.: Toward improved calibration of hydrologic models: Multiple and  
793 noncommensurable measures of information, *Water Resour. Res.*, 34, 751–763, 1998.
- 794 Gupta, H. V., Bastidas, L. A., Vrugt, J. A., and Sorooshian, S.: Multiple criteria global optimization for watershed  
795 model calibration, *Water Sci. Appl.*, 6, 125–132, 2003.
- 796 Gupta, H. V., Clark, M. P., Vrugt, J. A., Abramowitz, G., and Ye, M.: Towards a comprehensive assessment of  
797 model structural adequacy, *Water Resour. Res.*, 48, W08301, doi:10.1029/2011WR011044, 2012.
- 798 Hock, R.: Temperature index melt modelling in mountain areas, *J. Hydrol.*, 282, 104–115, 2003.
- 799 | Hublart, P., Ruelland, D., Dezetter, A., and Jourde, H.: [ModelingModelling](#) current and future trends in water  
800 availability for agriculture on a semi-arid and mountainous Chilean catchment, in: *Cold and Mountain  
801 Region Hydrological Systems Under Climate Change: Towards Improved Projections*, IAHS-AISH P., 360,  
802 26–32, 2013.
- 803 Hublart, P., Ruelland, D., Dezetter, A., and Jourde, H.: Assessing the capacity to meet irrigation water needs for  
804 viticulture under climate variability in the Chilean Andes, in: *Hydrology in a Changing World:  
805 Environmental and Human Dimensions*, Proc. 7th FRIEND Int. Conf., Montpellier, France, 24–28 February  
806 2014, IAHS-AISH P., 363, 209–214, 2014.
- 807 Hublart, P., Ruelland, D., García de Cortázar Atauri, I., and Ibacache, A.: Assessing the reliability of conceptual  
808 hydrological [modelingmodelling](#) in a cultivated, drought-prone catchment of the Chilean Andes, in:  
809 *Hydrologic Non-Stationarity and Extrapolating Models to Predict the Future*, IAHS-AISH P. (in press),  
810 2015.
- 811 Huisman, J. A., Rings, J., Vrugt, J. A., Sorg, J., Vereecken, H.: Hydraulic properties of a model dike from  
812 coupled Bayesian and multi-criteria hydrogeophysical inversion, *J. Hydrol.*, 380, 62–73, 2010.
- 813 IPCC: Full Report: the Physical Science Basis, in: *Contribution of Working Group I to the Fifth Assessment  
814 Report of the Intergovernmental Panel on Climate Change*, Climate Change 2013, edited by: Stocker, T. F.,  
815 Qin, D., Plattner, G.-K., Tignor, M., Allen, S. K., Boschung, J., Nauels, A., Xia, Y., Bex, V., and Midgley, P.  
816 M., Cambridge University Press, Cambridge, UK and New York, NY, USA, 1261–1264, 2013.
- 817 Jakeman, A. J. and Hornberger, G. M.: How much complexity is warranted in a rainfall-runoff model?, *Water  
818 Resour. Res.*, 29, 2637–2649, 1993.
- 819 Jakeman, A. J., and Letcher, R. A.: Integrated assessment and modelling: features, principles and examples for  
820 catchment management, *Environ. Modell. Softw.*, 18, 491–501, 2003.

- 821 Jothityangkoon, C., Sivapalan, M., and Farmer, D. L.: Process controls of water balance variability in a large  
822 semi-arid catchment: downward approach to hydrological model development, *J. Hydrol.*, 254, 174–198,  
823 2001.
- 824 Jourde, H., Rochette, R., Blanc, M., Brisset, N., Ruelland, D., Freixas, G., and Oyarzun, R. : Relative  
825 contribution of groundwater and surface water fluxes in response to climate variability of a mountainous  
826 catchment in the Chilean Andes, in: *Cold Regions Hydrology in a Changing Climate*, IAHS-AISH P., 346,  
827 180–188, 2011.
- 828 Kalthoff, N., Fiebig-Wittmaack, M., Meißner, C., Kohler, M., Uriarte, M., Bischoff-Gauß, I., and Gonzales, E.:  
829 The energy balance, evapo-transpiration and nocturnal dew deposition of an arid valley in the Andes, *J.*  
830 *Arid Environ.*, 65, 420–443, 2006.
- 831 Kavetski, D., and Kuczera, G.: Model smoothing strategies to remove microscale discontinuities and spurious  
832 secondary optima in objective functions in hydrological calibration, *Water Resour. Res.*, 43, W03411, ,  
833 doi:10.1029/2006WR005195, 2007.
- 834 | Kavetski, D., and Fenicia, F.: Elements of a flexible approach for conceptual hydrological **modelingmodelling**: 2.  
835 Application and experimental insights, *Water Resour. Res.*, 47, W11511, doi:10.1029/2011WR010748,  
836 2011.
- 837 Khu, S. T., and Madsen, H.: Multiobjective calibration with Pareto preference ordering: An application to  
838 rainfall-runoff model calibration, *Water Resour. Res.*, 41, W03004, 10.1029/2004WR003041, 2005.
- 839 Kiptala, J. K., Mul, M. L., Mohamed, Y. A. and van der Zaag, P.: Modelling stream flow and quantifying blue  
840 water using a modified STREAM model for a heterogeneous, highly utilized and data-scarce river basin in  
841 Africa, *Hydrol. Earth Syst. Sci.*, 18, 2287–2303, 2014.
- 842 Kirchner, J. W.: Getting the right answers for the right reasons: Linking measurements, analyses, and models to  
843 advance the science of hydrology, *Water Resour. Res.*, 42, WR004362, doi:10.1029/2005WR004362, 2006.
- 844 Kokkonen, T. S., and Jakeman, A. J.: A comparison of metric and conceptual approaches in rainfall-runoff  
845 **modelingmodelling** and its implications, *Water Resour. Res.*, 37, 2345–2352, 2001.
- 846 Krueger, T., Freer, J., Quinton, J. N., Macleod, C. J. A., Bilotta, G. S., Brazier, R. E., Butler, P., and Haygarth, P.  
847 M.: Ensemble evaluation of hydrological model hypotheses, *Water Resour. Res.*, 46, W07516.  
848 doi:10.1029/2009WR007845, 2010.
- 849 Lee, G., Tachikawa, Y., and Takara, K.: Comparison of model structural uncertainty using a multi-objective  
850 optimization method, *Hydrol. Process.*, 25, 2642–2653, 2011.
- 851 Madsen, H.: Automatic calibration of a conceptual rainfall–runoff model using multiple objectives, *J. Hydrol.*,  
852 235, 276–288, 2000.
- 853 MacDonell, S., Kinnard, C., Mölg, T., Nicholson, L., and Abermann, J.: Meteorological drivers of ablation  
854 processes on a cold glacier in the semiarid Andes of Chile, *The Cryosphere*, 7, 1833–1870, doi:10.5194/tc-  
855 7-1513-2013, 2013.
- 856 McDonnell, J. J., Sivapalan, M., Vaché, K., Dunn, S., Grant, G., Haggerty, R., Hinz, C., Hooper, R., Kirchner, J.,  
857 Roderick, M. L., Selker, J., and Weiler, M.: Moving beyond heterogeneity and process complexity: A new  
858 vision for watershed hydrology, *Water Resour. Res.*, 43, W07301, doi:10.1029/2006WR005467, 2007.
- 859 McMillan, H.: Effect of spatial variability and seasonality in soil moisture on drainage thresholds and fluxes in a  
860 conceptual hydrological model, *Hydrol. Process.*, 26, 2838–2844, doi: 10.1002/hyp.9396, 2012a.
- 861 McMillan, H., Tetzlaff, D., Clark, M., and Soulsby, C.: Do time-variable tracers aid the evaluation of  
862 hydrological model structure? A multimodel approach, *Water Resour. Res.*, 48, W05501,  
863 doi:10.1029/2011WR011688, 2012b.
- 864 Michaud, J., and Sorooshian, S.: Comparison of simple versus complex distributed runoff models on a semi-arid  
865 watershed, *Water Resour. Res.*, 30, 593–605, 1994.
- 866 | Milano, M., Ruelland, D., Dezetter, A., Fabre, J., Ardoin-Bardin, S., and Servat, E.: **ModelingModelling** the  
867 current and future capacity of water resources to meet water demands in the Ebro basin, *J. Hydrol.*, 500,  
868 114–126, 2013.
- 869 Minville, M., Brissette, F., and Leconte, R.: Uncertainty of the impact of climate change on the hydrology of a  
870 nordic watershed, *J. Hydrol.*, 358, 70–83, 2008.

- 871 Montecinos, A. and Aceituno, P.: Seasonality of the ENSO-Related Rainfall Variability in Central Chile and  
872 Associated Circulation Anomalies, *J. Climate*, 16, 281–296, 2003. Moore, R. J.: The PDM rainfall-runoff  
873 model, *Hydrol. Earth Syst. Sci.*, 11, 483–499, 2007.
- 874 Oudin, L., Hervieu, F., Michel, C., Perrin, C., Andréassian, V., Anctil, F., and Loumagne, C.: Which potential  
875 evapotranspiration input for a lumped rainfall-runoff model?: Part 2—Towards a simple and efficient  
876 potential evapotranspiration model for rainfall-runoff modelling, *J. Hydrol.*, 303, 290–306, 2005.
- 877 Parajka, J., and Blöschl, G.: The value of MODIS snow cover data in validating and calibrating conceptual  
878 hydrologic models, *J. Hydrol.*, 358, 240–258, 2008.
- 879 Pellicciotti, F., Helbing, J., Rivera, A., Favier, V., Corripio, J., Araos, J., Sicart, J.-E. and Carenzo, M.: A study of  
880 the energy balance and melt regime on Juncal Norte Glacier, semi-arid Andes of central Chile, using melt  
881 models of different complexity, *Hydrol. Process.*, 22, 3980–3997. doi: 10.1002/hyp.7085, 2008.
- 882 Perrin, C., Michel, C., and Andréassian, V.: Improvement of a parsimonious model for streamflow simulation, *J.*  
883 *Hydrol.*, 279, 275–289, 2003.
- 884 Pourrier, J., Jourde, H., Kinnard, C., Gascoïn, S., and Monnier, S.: Glacier meltwater flow paths and storage in a  
885 geomorphologically complex glacial foreland: The case of the Tapado glacier, dry Andes of Chile (30° S), *J.*  
886 *Hydrol.*, 519, 1068–1083, doi:10.1016/j.jhydrol.2014.08.023, 2014.
- 887 Quintana, J. M. and Aceituno, P.: Changes in the rainfall regime along the extratropical west coast of South  
888 America (Chile): 30–43°S, *Atmósfera*, 25, 1–22, 2012.
- 889 Refsgaard, J. C., and Knudsen, J.: Operational validation and intercomparison of different types of hydrological  
890 models, *Water Resour. Res.*, 32, 2189–2202, 1996.
- 891 Ruelland, D., Brisset, N., Jourde, H., and Oyarzun, R.: Modelling the impact of climatic variability on the  
892 groundwater and surface flows from a mountainous catchment in the Chilean Andes, in: *Cold Regions*  
893 *Hydrology in a Changing Climate*, IAHS-AISH P., 346, 171–179, 2011.
- 894 Ruelland, D., Ardoin-Bardin, S., Collet, L., and Roucou, P.: Simulating future trends in hydrological regime of a  
895 large Sudano-Sahelian catchment under climate change, *J. Hydrol.*, 424–425, 207–216, 2012.
- 896 Ruelland, D., Dezetter, A., and Hublart, P.: Sensitivity analysis of hydrological modelling to climate forcing in a  
897 semi-arid mountainous catchment, in: *Hydrology in a Changing World: Environmental and Human*  
898 *Dimensions*, Proc. 7th FRIEND Int. Conf., Montpellier, France, 24–28 February 2014, IAHS-AISH P., 363,  
899 145–150, 2014.
- 900 Savenije, H. H. G.: HESS Opinions "The art of hydrology", *Hydrol. Earth Syst. Sci.*, 13, 157–161,  
901 doi:10.5194/hess-13-157-2009, 2009.
- 902 Schaeffli, B., Harman, C. J., Sivapalan, M., and Schymanski, S. J.: HESS Opinions: Hydrologic predictions in a  
903 | changing environment: behavioral [modelingmodelling](#), *Hydrol. Earth Syst. Sci.*, 15, 635–646,  
904 doi:10.5194/hess-15-635-2011, 2011.
- 905 Schreider, S., Whetton, P. H., Jakeman, A. J., and Pittock, A. B.: Runoff modelling for snow-affected catchments  
906 in the Australian alpine region, eastern Victoria, *J. Hydrol.*, 200, 1–23, 1997.
- 907 Seibert, J.: Multi-criteria calibration of a conceptual runoff model using a genetic algorithm, *Hydrol. Earth Syst.*  
908 *Sci.*, 4, 215–224, doi:10.5194/hess-4-215-2000, 2000.
- 909 Seibert, J. and McDonnell, J. J.: On the dialog between experimentalist and modeler in catchment hydrology:  
910 Use of soft data for multicriteria model calibration, *Water Resour. Res.*, 38, W01241, doi:  
911 10.1029/2001WR000978, 2002.
- 912 | Seibert, J. and Vis, M. J. P.: Teaching hydrological [modelingmodelling](#) with a user-friendly catchment-runoff-  
913 model software package, *Hydrol. Earth Syst. Sci.*, 16, 3315–3325, 2012.
- 914 Shafii, M. and De Smedt, F.: Multi-objective calibration of a distributed hydrological model (WetSpa) using a  
915 genetic algorithm, *Hydrol. Earth Syst. Sci.*, 13, 2137–2149, 2009.
- 916 Sivapalan, M., Blöschl, G., Zhang, L., and Vertessy, R.: Downward approach to hydrological prediction, *Hydrol.*  
917 *Process.*, 17, 2101–2111, 2003.
- 918 Sivapalan, M.: Pattern, process and function: elements of a unified theory of hydrology at the catchment scale,  
919 *Encyclopedia of Hydrological Sciences*, doi:10.1002/0470848944.hsa012, online first, 2006.
- 920 Smith, T. J., and Marshall, L. A.: Exploring uncertainty and model predictive performance concepts via a

921 | modular snowmelt-runoff [modelingmodelling](#) framework, *Environ. Modell. Softw.*, 25, 691–701, 2010.

922 | Son, K., and Sivapalan, M.: Improving model structure and reducing parameter uncertainty in conceptual water  
923 | balance models through the use of auxiliary data, *Water Resour. Res.*, 43, W01415,  
924 | doi:10.1029/2006WR005032, 2007.

925 | Souvignet, M: Climate Change Impacts on Water Availability in the Semiarid Elqui Valley, Chile, Ph.D. thesis,  
926 | Cologne University of Applied Sciences, Institute for Technology in the Tropics, 110 pp., 2007.

927 | Souvignet, M., Hartmut, G., Lars, R., Kretschmer, N., and Oyarzún, R.: Statistical downscaling of precipitation  
928 | and temperature in north-central Chile: an assessment of possible climate change impacts in an arid Andean  
929 | watershed, *Hydrol. Sci. J.*, 55, 41–57, 2010.

930 | Squeo, F. A., Veit, H., Arancio, G., Gutiérrez, J. R., Arroyo, M. T. K., and Olivares, N.: Spatial heterogeneity of  
931 | high mountain vegetation in the Andean desert zone of Chile (30°S), *Mt. Res. Dev.*, 13, 203–209, 1993.

932 | Staudinger, M., Stahl, K., Seibert, J., Clark, M. P., and Tallaksen, L. M.: Comparison of hydrological model  
933 | structures based on recession and low flow simulations, *Hydrol. Earth Syst. Sci.*, 15, 3447–3459,  
934 | doi:10.5194/hess-15-3447-2011, 2011.

935 | Strauch, G., Oyarzun, J., Fiebig-Wittmaack, M., González, E., and Weise, S. M.: Contributions of the different  
936 | water sources to the Elqui river runoff (northern Chile) evaluated by H/O isotopes, *Isot. Environ. Health S.*,  
937 | 42, 303–322, 2006.

938 | Verbist, K., Robertson, A. W., Cornelis, W. M., and Gabriels, D.: Seasonal predictability of daily rainfall  
939 | characteristics in central northern Chile for dry-land management, *J. Appl. Meteorol. Clim.*, 49, 1938–1955,  
940 | 2010.

941 | Vicuña, S., Garreaud, R., and McPhee, J.: Climate change impacts on the hydrology of a snowmelt driven basin  
942 | in semiarid Chile, *Climatic Change*, 105, 469–488, 2011.

943 | Wagener, T., Lees, M. J., and Wheeler, H. S.: A toolkit for the development and applications of parsimonious  
944 | hydrological models, in: *Mathematical Models of Large Watershed Hydrology*, vol. 1, edited by: Singh, V.  
945 | P. and Frevert, D., Water Resources Publishers, Highland Ranch, CO, 87–136, 2002.

946 | Wainwright, J., and Mulligan, M. (Eds): *Environmental modelling – Finding simplicity in complexity*.  
947 | Chichester, John Wiley & Sons, Ltd., 2004.

948 | Xu, C.-Y., and Singh, V. P.: Review on regional water resources assessment models under stationary and  
949 | changing climate, *Water Resour. Manage.*, 18, 591–612, 2004.

950 | Young, G., Zavala, H., Wandel, J., Smit, B., Salas, S., Jimenez, E., Fiebig, M., Espinoza, R., Diaz, H., and  
951 | Cepeda, J.: Vulnerability and adaptation in a dryland community of the Elqui Valley, Chile, *Climatic*  
952 | *Change*, 98, 245–276, 2010.

953

954 TABLES & CAPTIONS

955

956 | **Table 1.** Constitutive equations of fluxes between the various components of the [modelingmodelling](#) options  
 957 | described in Fig. 23. Parameter (in italic) significations and units are detailed in Table 2. P: catchment-averaged  
 958 | daily precipitation; Rain: rain fraction of precipitation P; Snow: snow fraction of precipitation P; T: catchment-  
 959 | averaged daily temperature; PE: catchment-averaged daily potential evapotranspiration; AE: catchment-averaged  
 960 | daily actual evapotranspiration;  $S_j, j \in [1,5]$ : state variables of the conceptual stores;  $Q_j, j \in [1,5]$ : water fluxes  
 961 | between the model components).

Options	Constitutive equations	Options	Constitutive equations
A1	$\text{Snow} = P / (1 + \exp[(T - T_S) / m_S])$ $\text{Rain} = P - \text{Snow}$	C3	$Q_1 = (\text{Melt} + \text{Rain}) [1 - (1 - S_1 / S_m)^b]$ $Q_2 = K_1 S_1$
B1a, B1b, B1c	$\text{Melt} = MF (\bar{T} - \log[1 + \exp(-\bar{T})])$ with $\bar{T} = (T - T_M) / m_M$ and $m_M = 0.1^\circ\text{C}$	D1	$Q_3 = Q_2$ and $Q_4 = Q_1$ or $Q_3 = Q_1$
B1a	$MF = f_M m_M$	D2	$Q_3 = Q_1 + Q_2$
B1b	$MF = r_1 + r_2 T_{30}$ with $T_{30}$ the mean temperature of the last 30 days	D3	$Q_3 = (1 - \alpha) Q_1$ $Q_4 = \alpha Q_1$
B1c	$MF = f_1 + f_2 \sin(0.551\pi + 2\pi d / 366)$	E1	$Q_{j,\text{lag}} = Q_2$ with $j \in \{3,4\}$
C1	$AE = \min(\text{Melt} + \text{Rain}, K_C PE)$	E2	$Q_{j,\text{lag}}(t) = \sum_{i=1}^{N_b} \omega(i) Q_j(t - i + 1)$ with $\omega(i) = \int_{i-1}^i 2udu / N_b^2$
C2, C3	$AE = PE \min(1, S_1 / S_m)$	F1a, F2a, F3a	$Q_5 = K_2 S_2^{1+\delta}$ $Q_6 = K_3 S_3$
C1	$Q_1 = \text{Melt} + \text{Rain}$	F1b, F2b, F3b	$Q_5 = K_4 S_2 + K_2 (\bar{S}_2 - \log[1 + \exp(-\bar{S}_2)])$ $Q_6 = K_3 S_3$ with $\bar{S}_2 = (S_2 - S_C) / m_C$ and $m_C = 0.1 \text{ mm}^{-1}$
C2	$Q_1 = (\text{Melt} + \text{Rain}) (S_1 / S_m)^\beta$	F3a, F3b	$Q_6 = DS_2$

962

963 | **Table 2.** Parameters used in the various modelingmodelling options with their signification and initial  
964 sampling. (\*) The possible values for  $K_C$  were limited to a maximum of 0.5 to reflect the extreme aridity of  
965 the catchment.  
966

Parameter	Options	Signification	Units	Initial range
$T_S$	A1	Rain / snow partitioning temperature threshold	°C	-10 – 10
$m_S$	A1	Rain / snow partitioning smoothing parameter	–	0.01 – 3
$T_M$	B1a, B1b, B1c	Snowmelt temperature threshold	°C	-10 – 10
$f_M$	B1a	Constant melt factor	°C.mm <sup>-1</sup>	0 – 10
$r_1$	B1b	Coefficient for computation of the variable melt factor	°C.mm <sup>-1</sup>	1 – 5
$r_2$	B1b	Coefficient for computation of the variable melt factor	°C.mm <sup>-1</sup>	1 – 5
$f_1$	B1c	Coefficient for computation of the variable melt factor	°C.mm <sup>-1</sup>	1 – 5
$f_2$	B1c	Coefficient for computation of the variable melt factor	°C.mm <sup>-1</sup>	1 – 5
$K_C$	C1	Evapotranspiration coefficient	–	0.05 – 0.5 (*)
$S_m$	C2, C3	Maximum storage capacity of the moisture-accounting store	mm	10 – 100
$\beta$	C2	Shape parameter	–	0.1 – 3
$b$	C3	Shape parameter of Pareto distribution	–	0.1 – 3
$K_1$	C3	Infiltration coefficient	d <sup>-1</sup>	0.001 – 0.7
$\alpha$	D3	Splitting parameter	–	0.1 – 0.9
$N_b$	E2	Number of time steps in the lag routine	–	1 – 6
$K_2$	F1a to F3b	Storage coefficient	d <sup>-1</sup>	0.01 – 0.99
$K_3$	F1a to F3b	Storage coefficient	d <sup>-1</sup>	0.001 – 0.01 (F1a, F1b, F3a, F3b) 0.001 – 0.1 (F2a, F2b)
$\delta$	F1a, F2a, F3a	Power law parameter of the non-linear store in the runoff transformation module	–	0 – 1
$S_c$	F1b, F2b, F3b	Threshold parameter of the non-linear store in the runoff transformation module	mm	10 – 300
$D$	F3a, F3b	Recharge coefficient	d <sup>-1</sup>	0.001 – 0.5
$K_4$	F1b, F2b, F3b	Storage coefficient	d <sup>-1</sup>	0.001 – 0.01

967

968 **Table 3.** Coordinates of the cluster centroids in the four-dimensional (4D) space of performance measures. The  
 969 number of models with membership values > 50% ( $N_{50\%}$ ) is given for each cluster.  
 970

Calibration period (1997–2011)					
Cluster no.	Crit1 (1-NSE)	Crit2 (1-NSE <sub>log</sub> )	Crit3 (VE <sub>M</sub> ) (%)	Crit4 (SE) (%)	N <sub>50%</sub>
1	0.15	0.25	10	9	24
2	0.23	0.30	10	10	24
3	0.49	0.58	23	11	10
4	0.60	0.62	25	16	13
5	0.92	0.97	33	20	1

Validation period (1982–1996)					
Cluster no.	Crit1 (1-NSE)	Crit2 (1-NSE <sub>log</sub> )	Crit3 (VE <sub>M</sub> ) (%)	Crit4 (VE <sub>C</sub> ) (%)	N <sub>50%</sub>
1	0.24	0.21	14	3	15
2	0.32	0.29	15	4	25
3	0.38	0.31	15	5	8
4	0.51	0.42	25	23	8
5	0.61	0.44	27	27	11
6	0.61	0.51	30	33	5

971

972 **Table 4.** Detailed composition of Clusters 1 in calibration and validation. The tables indicate the numbers and  
973 the names of the models as well as their number of parameters NP. For each criterion only the best performance  
974 value obtained along the Pareto front is given.  $N_{\text{par}}$  (%) represents the proportion of observations enclosed within  
975 the simulation bounds of each Pareto set of solutions. Asterisks are used to indicate the models which are not in  
976 the best-performing group (Cluster 1) either in calibration or in validation.  
977

Calibration period (1997–2011)							
Model no.	Model name (options)	NP	NSE	NSE <sub>log</sub>	VE <sub>M</sub> (%)	SE (%)	$N_{\text{par}}$ (%)
2	A1–B1a–C1–D1–E1–F2b	9	0.87	0.76	10.6	11.2	76.0
4	A1–B1a–C1–D1–E1–F3b	10	0.84	0.77	10.4	11.2	53.2
8	A1–B1a–C1–D3–E2–F2b	11	0.83	0.75	11.7	11.1	76.5
20	A1–B1a–C3–D1–E2–F2b	12	0.83	0.76	10.0	11.4	60.0
22	A1–B1a–C3–D2–E1–F2b	11	0.90	0.77	10.4	11.2	64.1
26	A1–B1b–C1–D1–E1–F2b	10	0.87	0.77	10.1	11.5	58.4
30 (*)	A1–B1b–C1–D3–E2–F1b	12	0.84	0.70	9.8	11.4	69.6
32 (*)	A1–B1b–C1–D3–E2–F2b	12	0.83	0.71	11.1	11.4	68.4
44	A1–B1b–C3–D1–E2–F2b	13	0.89	0.77	10.6	11.4	63.4
46	A1–B1b–C3–D2–E1–F2b	12	0.90	0.76	10.7	11.4	45.4
49 (*)	A1–B1c–C1–D1–E1–F2a	9	0.82	0.73	10.9	7.0	67.0
50	A1–B1c–C1–D1–E1–F2b	10	0.86	0.77	10.4	7.0	67.4
52 (*)	A1–B1c–C1–D1–E1–F3b	11	0.85	0.72	8.8	8.1	65.7
53 (*)	A1–B1c–C1–D3–E2–F1a	11	0.79	0.76	10.8	7.0	63.8
54	A1–B1c–C1–D3–E2–F1b	12	0.90	0.78	11.5	7.5	55.7
55 (*)	A1–B1c–C1–D3–E2–F2a	11	0.80	0.73	10.7	7.0	54.5
56	A1–B1c–C1–D3–E2–F2b	12	0.85	0.75	10.8	7.6	76.3
65	A1–B1c–C3–D1–E2–F1a	12	0.83	0.78	8.0	7.7	65.0
66 (*)	A1–B1c–C3–D1–E2–F1b	13	0.81	0.77	9.6	6.8	63.5
67 (*)	A1–B1c–C3–D1–E2–F2a	12	0.81	0.75	10.7	7.0	73.7
68	A1–B1c–C3–D1–E2–F2b	13	0.85	0.74	10.6	6.8	74.5
69 (*)	A1–B1c–C3–D2–E1–F2a	11	0.82	0.73	10.6	7.0	51.8
70	A1–B1c–C3–D2–E1–F2b	12	0.87	0.76	10.7	7.5	76.4
72 (*)	A1–B1c–C3–D2–E1–F3b	13	0.81	0.71	9.8	7.1	69.0

978  
979

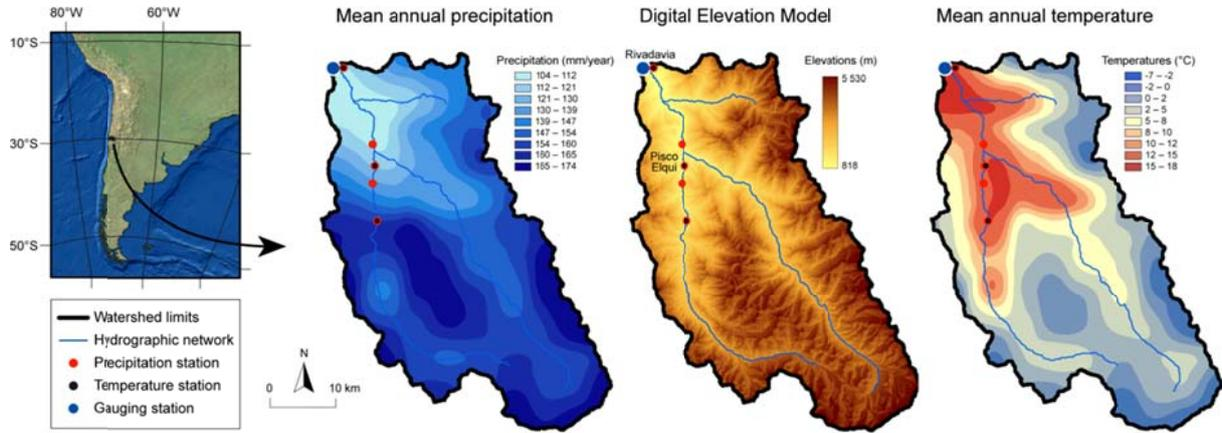
Validation period (1982–1996)							
Model no.	Model name	NP	NSE	NSE <sub>log</sub>	VE <sub>M</sub> (%)	VE <sub>C</sub> (%)	$N_{\text{par}}$ (%)
2	A1–B1a–C1–D1–E1–F2b	9	0.75	0.78	13.3	2.7	87.1
4	A1–B1a–C1–D1–E1–F3b	10	0.73	0.80	14.1	3.8	50.0
8	A1–B1a–C1–D3–E2–F2b	11	0.75	0.76	14.5	5.8	84.8
20	A1–B1a–C3–D1–E2–F2b	12	0.72	0.77	13.7	3.7	58.4
22	A1–B1a–C3–D2–E1–F2b	11	0.76	0.78	12.3	3.3	75.3
26	A1–B1b–C1–D1–E1–F2b	10	0.74	0.78	12.9	3.5	70.2
42 (*)	A1–B1b–C3–D1–E2–F1b	13	0.73	0.75	15.6	3.3	62.7
44	A1–B1b–C3–D1–E2–F2b	13	0.74	0.79	13.0	4.1	69.3
46	A1–B1b–C3–D2–E1–F2b	12	0.76	0.77	15.2	3.4	48.4
50	A1–B1c–C1–D1–E1–F2b	10	0.78	0.81	13.9	2.5	73.1
54	A1–B1c–C1–D3–E2–F1b	12	0.77	0.78	15.3	3.5	60.8
56	A1–B1c–C1–D3–E2–F2b	12	0.75	0.77	13.2	4.5	81.3
65	A1–B1c–C3–D1–E2–F1a	12	0.74	0.80	13.8	3.6	73.0
68	A1–B1c–C3–D1–E2–F2b	13	0.77	0.74	13.5	3.7	78.7
70	A1–B1c–C3–D2–E1–F2b	12	0.73	0.78	14.2	3.4	79.4

980

981 **FIGURES & CAPTIONS**

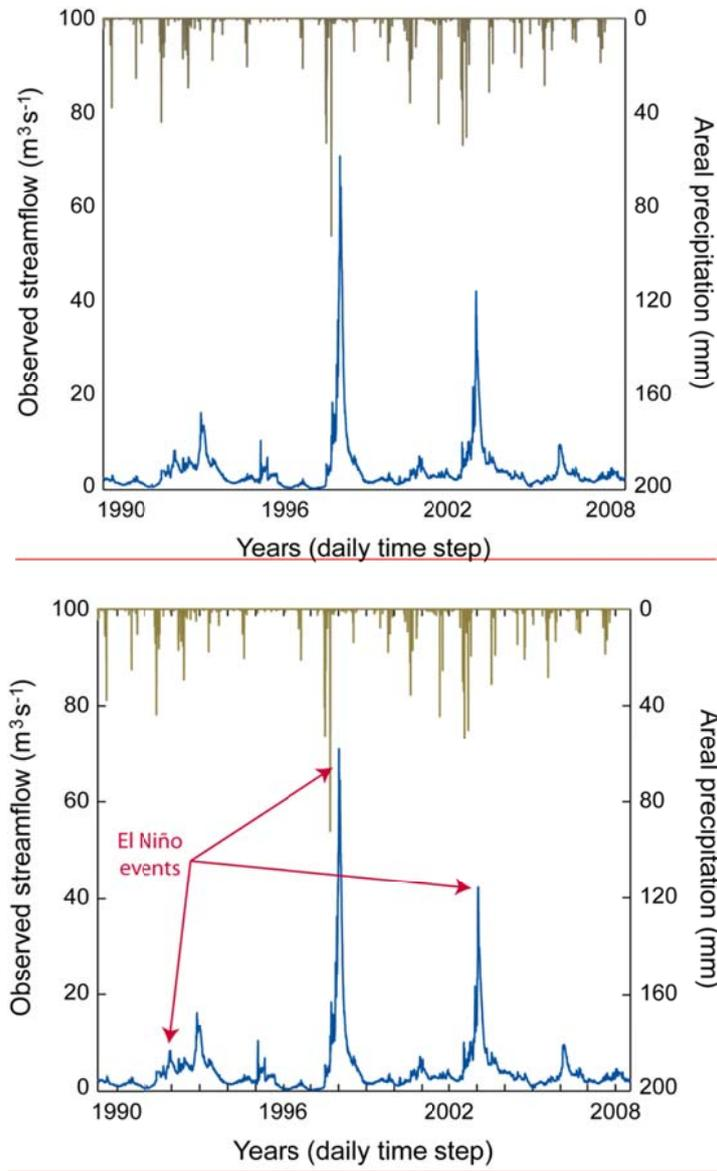
982

983 **Figure 1.** The Claro River Basin at Rivadavia (1515 km<sup>2</sup>) in Chile: topography and mean annual precipitation  
984 and temperature over 1982–2011 (based on Ruelland *et al.*, 2014). Several of the stations used in this study were  
985 located outside the catchment and therefore not displayed on the following maps.



986

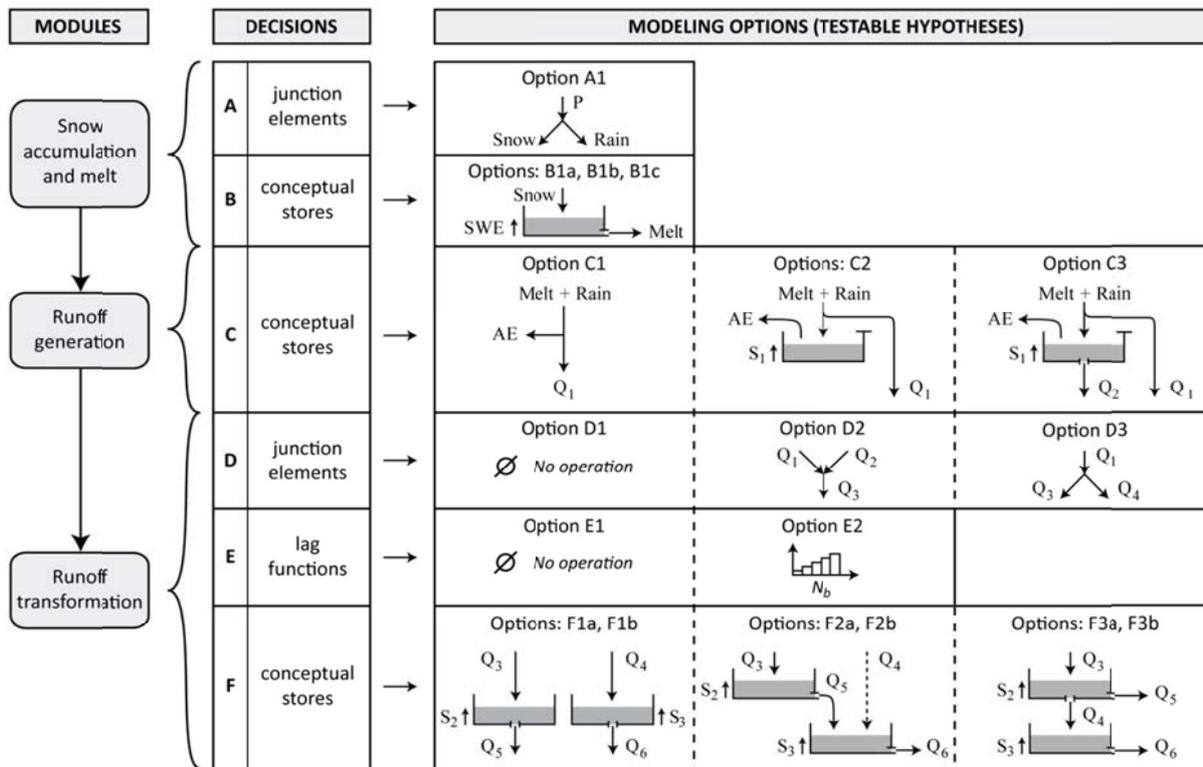
987 **Figure 2.** Interannual variability in precipitation and observed streamflow from 1989 to 2008. The hydrological  
988 year was defined from May to April so as to capture the snowmelt and peak flow seasons at mid-year (the  
989 graduations on the x-axis indicate the 1<sup>st</sup> of January of each year). Streamflow values are those measured at the  
990 catchment outlet before accounting for water abstractions. Precipitation values are those obtained after  
991 interpolation.



992

993

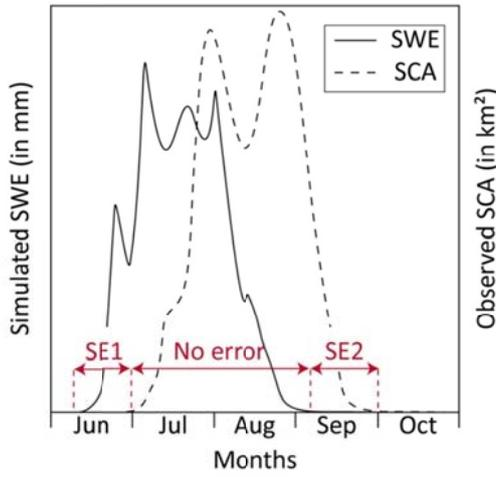
994 | **Figure 3.** Overall architecture (modules), decision tree and available **modelingmodelling** options of the  
 995 modular multiple-hypothesis framework (P: catchment-averaged daily precipitation; SWE: snow water  
 996 equivalent; AE: catchment-averaged daily actual evapotranspiration;  $S_j, j \in [1,5]$ : state variables of the  
 997 conceptual stores;  $Q_j, j \in [1,5]$ : water fluxes between the model components).



998

999  
 1000  
 1001  
 1002

**Figure 4.** Description of the snow error criterion. The overall snow error (SE) can be described as a sum of two terms, SE1 and SE2, whose values are given by a confusion matrix. In this example, water storage in the snow-accounting store (solid line) starts (SE1) and ends (SE2) sooner than what would be expected from the SCA data (dashed line).



Definition of the snow error (%):

$$\text{Crit4} = \text{SE} = \frac{1}{N_{\text{SCA}}} (\text{SE1} + \text{SE2})$$

with  $N_{\text{SCA}}$  the number of days with available SCA observations

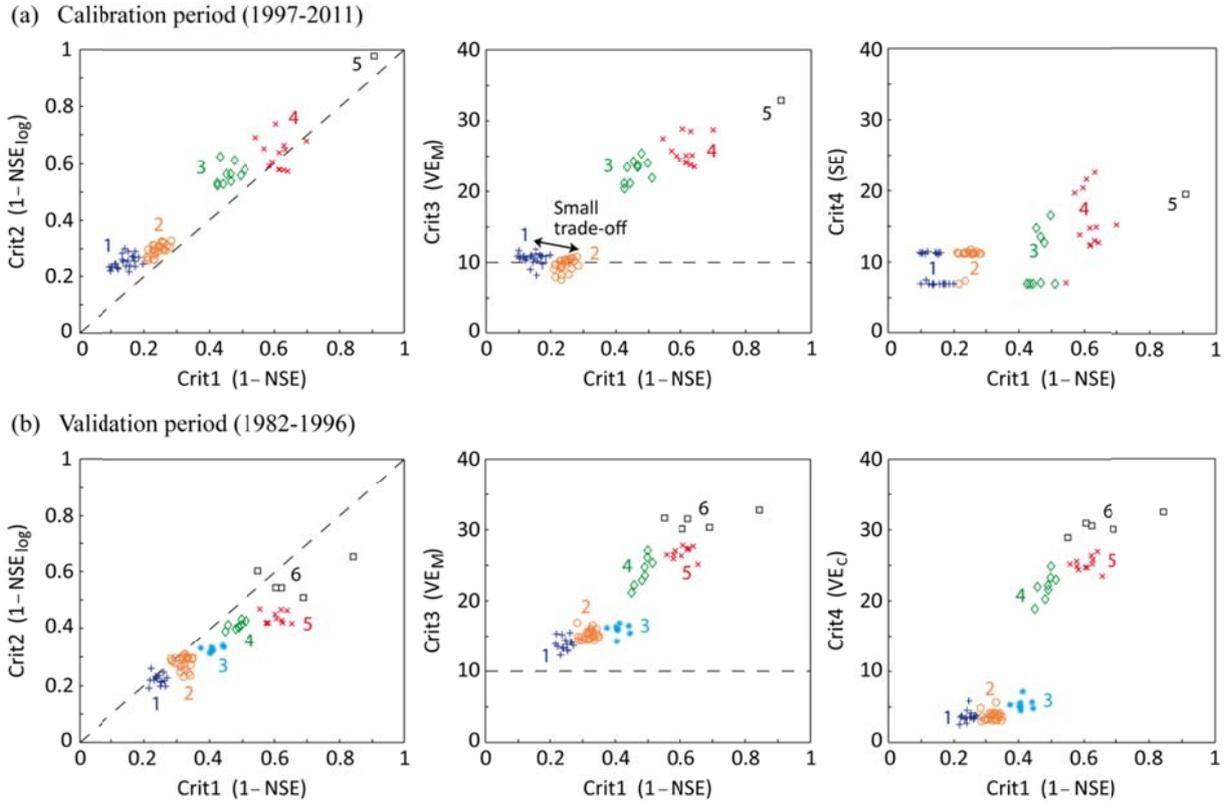
Confusion matrix (days) of the SE:

		SWE	
		> 0	= 0
SCA	> 0	No error	SE2
	= 0	SE1	No error

1003

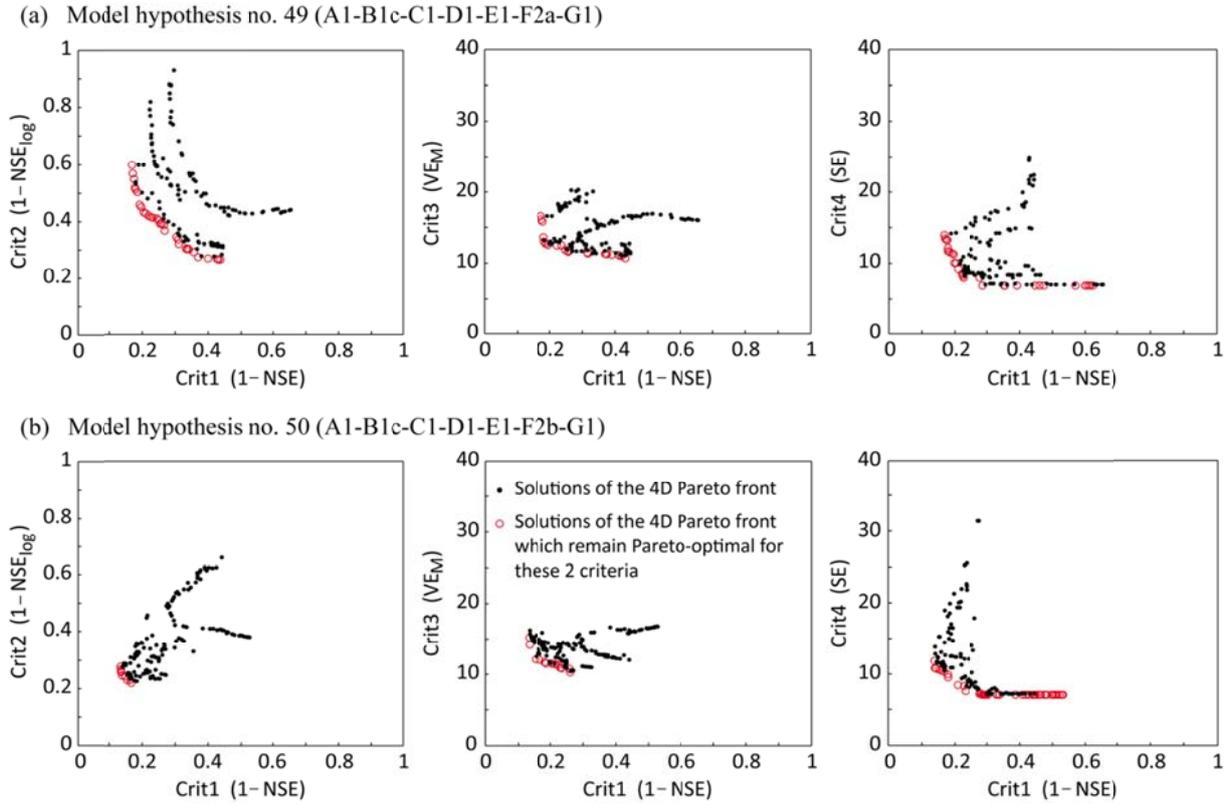
1004  
1005  
1006

**Figure 5.** Projections of the clusters onto three possible planes of the objective space in calibration and validation. As explained in Sect 3.3., each point represents a different model hypothesis.



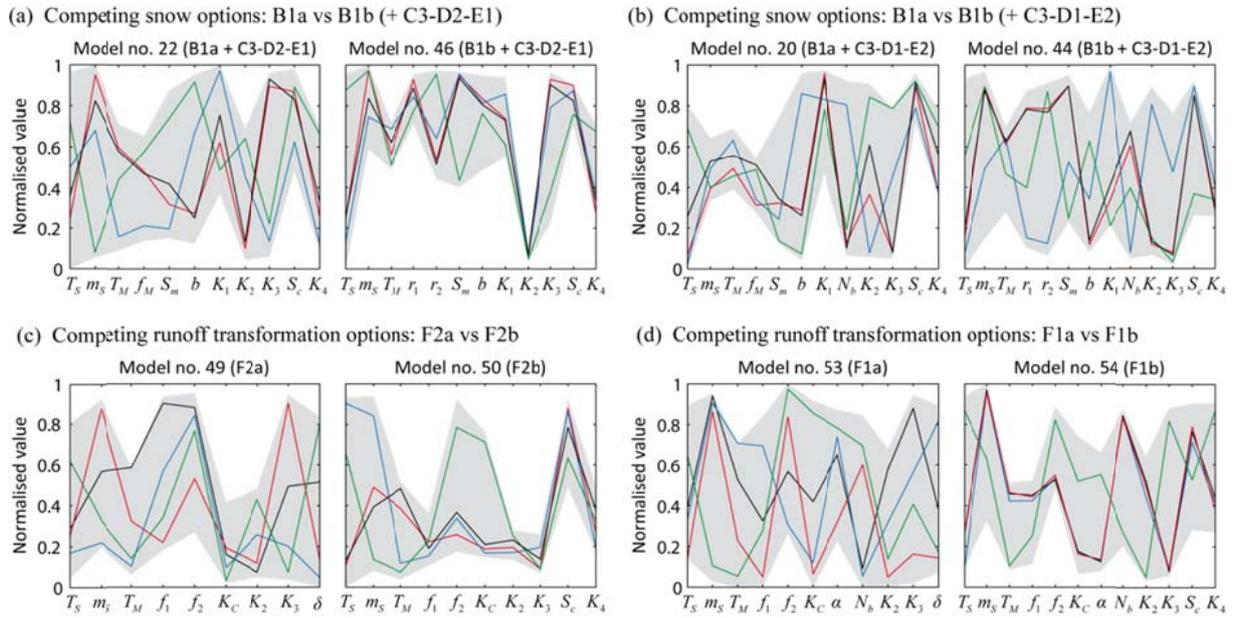
1007

1008 **Figure 6.** Projections of the Pareto fronts of model hypotheses (a) no. 49 (A1-B1c-C1-D1-E1-F2a) and (b) no.  
 1009 50 (A1-B1c-C1-D1-E1-F2b) onto three possible two-dimensional subspaces of the objective space.



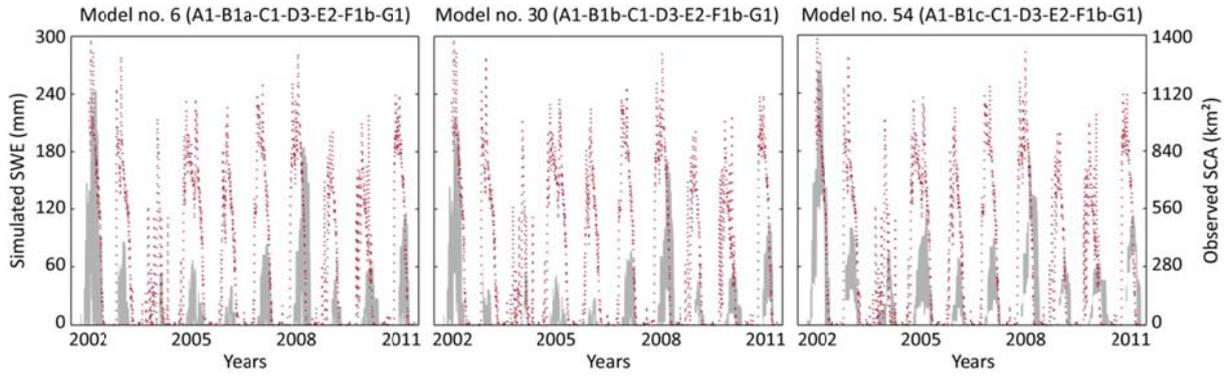
1010

1011 **Figure 7.** Estimated normalized ranges of the Pareto-optimal sets of eight alternative model structures differing  
 1012 in at least one of their components. The colored lines stand for the best solutions obtained in calibration with  
 1013 respect to the high flow criterion (in black), the low flow criterion (in red), the mean annual volume error (in  
 1014 blue) and the snow error (in green).  
 1015



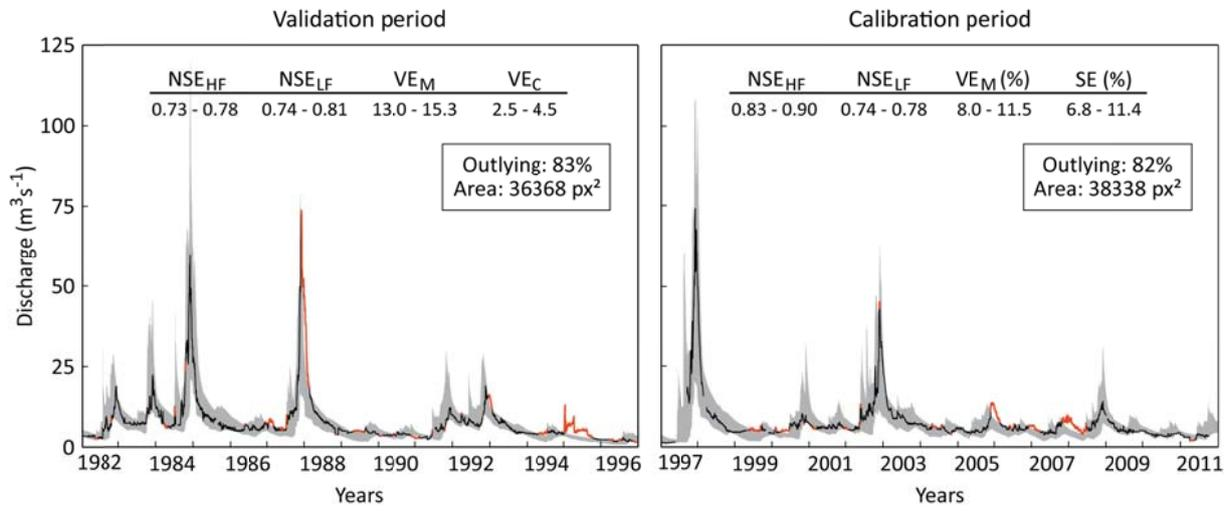
1016

1017 **Figure 8.** Comparison of MODIS-based SCA data (red dashed lines) with the SWE simulations (shaded areas)  
1018 of models no. 6, 30 and 54. The shaded area corresponds to the range of SWE simulations obtained from the  
1019 Pareto sets of these models.



1020

1021 **Figure 9.** Comparison of observed daily discharge at Rivadavia with the overall uncertainty envelope obtained  
 1022 by combining the Pareto-envelopes of 8 model structures. These structures have been selected among the 14  
 1023 members of Cluster 1 in both calibration and validation so as to minimize the uncertainty envelope area (Area, in  
 1024 pixels<sup>2</sup>) while holding constant the number of outlying observations (Outlying, in %). The red parts indicate  
 1025 potential errors in the model structures or observed data.



1026